Since January 2020 Elsevier has created a COVID-19 resource centre with free information in English and Mandarin on the novel coronavirus COVID-19. The COVID-19 resource centre is hosted on Elsevier Connect, the company's public news and information website.

Computational Biology and Chemistry 98 (2022) 107657

Contents lists available at ScienceDirect

Computational Biology and Chemistry

journal homepage: www.elsevier.com/locate/cbac

Design and various in silico studies of the novel curcumin derivatives as potential candidates against COVID-19 -associated main enzymes

Hakan Alici [a,*], Hakan Tahtaci [b], Kadir Demir [a]

[a] Department of Physics, Faculty of Arts and Sciences, Zonguldak Bulent Ecevit University, 67100 Zonguldak, Turkey
[b] Department of Chemistry, Faculty of Science, Karabuk University, 78050 Karabuk, Turkey

ARTICLE INFO

Keywords:
Coronavirus
SARS-CoV-2
MM-PBSA
Curcumin
Docking
Drug design
Molecular dynamic
Simulation

ABSTRACT

The novel coronavirus disease (COVID-19) is a highly contagious disease caused by the SARS-CoV-2 virus, leading severe acute respiratory syndrome in patients. Although various antiviral drugs and their combinations have been tried so far against SARS-CoV-2 and they have shown some effectiveness, there is still a need for safe and cost-effective binding inhibitors in the fight against COVID-19. Therefore, phytochemicals in nature can be a quick solution due to their wide therapeutic spectrum and strong antiviral, anti-inflammatory, and antioxidant properties. In this context, the low toxicity, and high pharmacokinetic properties of curcumin, which is a natural phytochemical, as well as the easy synthesizing of its derivatives reveal the need for investigation of its various derivatives as inhibitors against coronaviruses. The present study focused on curcumin derivatives with reliable ADME profile and high molecular binding potency to different SARS-CoV-2 target enzymes (3CLPro, PLpro, NSP7/8/12, NSP7/8/12 +RNA, NSP15, NSP16, Spike, Spike+ACE). In the molecular docking studies, the best binding scores for the 22 proposed curcumin derivatives were obtained for the PLpro protein. Furthermore, MD simulations were performed for high-affinity ligand-PLpro protein complexes and subsequently, Lys157, Glu161, Asp164, Arg166, Glu167, Met208, Pro247, Pro248, Tyr264, Tyr273 and Asp302 residues of PLpro was determined to play key role for ligand binding by Molecular Mechanics Poisson-Boltzmann Surface Area (MM-PBSA) analysis. The results of the study promise that the proposed curcumin derivatives can be potent inhibitors against SARS-CoV-2 and be converted into pharmaceutical drugs. It is also expected that the findings may provide guiding insights to future design studies for synthesizing different antiviral derivatives of phytochemicals.

1. Introduction

The COVID-19, caused by the SARS-CoV-2 virus, first appeared in Wuhan, Hubei province of China, in December 2019 and lead to an unusual type of infectious pneumonia that causes severe acute respiratory syndromes in patients (Huang et al., 2020; Lu et al., 2020; Zu et al., 2020). Since the day of its pandemic situation, SARS-CoV-2 has caused 383,509,779 confirmed cases of infection, more than 5,693,824 deaths (WHO reports, 4 February 2022), and the number of newly infected and deaths is increasing day by day. For this reason, the whole world is trying to fight this coronavirus disease and scientific communities are researching for effective vaccines, drugs or treatments that can be used to combat COVID-19.

Although various antiviral drugs and their combinations have been tried for the treatment of COVID-19, no fully effective treatment has yet been found. The activity of coronaviruses can be restrained by inhibiting the virus's binding to human cell receptors, spreading and replication of their genetic material. In this context, studies on discovering new chemical drugs that will inhibit the enzyme proteins of coronaviruses continue at a great pace. In addition to these chemical drugs, satisfactory results have been also reported for various phytochemicals in the inhibition of coronaviruses (Gangadevi et al., 2021; Kumar et al., 2020; Mitra et al., 2021; Özdemir et al., 2020; Rajagopal et al., 2020; Singh et al., 2021; Vellingiri et al., 2020). Designing and discovering a new drug from scratch is a long process, and in this regard, derivatives of existing therapeutic molecules and phytochemicals with appropriate drug properties can be an effective and rapid solution to the COVID-19 crisis. To this end, there are a lot of theoretical efforts on COVID-19 focusing on natural compound (Adelusi et al., 2022; Badavath et al., 2020; Choudhary and Singh, 2022; Hasan et al., 2022; Mithilesh et al., 2022; Murugesan et al., 2021; Oluyori et al., 2022; Phong et al., 2022).

Curcuminoids are natural organic phytochemicals found in Turmeric

* Corresponding author.
E-mail address: hakanalici@beun.edu.tr (H. Alici).

https://doi.org/10.1016/j.compbiolchem.2022.107657
Received 9 July 2021; Received in revised form 4 February 2022; Accepted 25 February 2022
Available online 26 February 2022

(Curcuma longa) that are plant-derived and can be easily synthesized (Jennings and Parks, 2020; Sharifi-Rad et al., 2020). The main curcuminoids in commercial turmeric extracts are; consists of curcumin (77%), demethoxycurcumin (17%) and bisdemethoxycurcumin (6%) (Anand et al., 2007) and, as it is well known, curcumin is recognized as "Generally Recognized as Safe (GRAS)" by the Food and Drug Administration (FDA). It is well-established that curcuminoids are widely used in traditional medicine in Asia due to their anti-inflammatory and wound healing properties (Aggarwal et al., 2005; Cianciulli et al., 2016; Dai et al., 2018b; Kocaadam and Şanlier, 2017; Sidhu et al., 1998) and it has also been reported that they have anticancer (Astinfeshan et al., 2019; Kunnumakkara et al., 2017; Man et al., 2018; Yance and Sagar, 2006), antioxidant (Ak and Gülçin, 2008; Jovanovic et al., 1999), neuroprotective (Ganesh et al., 2017; Goozee et al., 2016), antimicrobial (Gupta and Ravishankar, 2005) properties and many other biological functions and activities (Badavath et al., 2016c; Jiang et al., 2017; Munigunti et al., 2014; Rahmani et al., 2016). Moreover, it has been shown that Curcumin can act as an anti-viral compound that inhibits replication of the virus in a wide range of RNA, DNA viruses (Ali and Banerjea, 2016; Balasubramanian et al., 2019; Dai et al., 2018a; Du et al., 2017; Ferreira et al., 2015; Gao et al., 2019; Huang et al., 2018; Jeong et al., 2015; Li et al., 2019; Lin et al., 2019; Mounce et al., 2017; Randazzo et al., 2016; Richart et al., 2018; von Rhein et al., 2016; Wu et al., 2015; Yang et al., 2016, 2017). It is also very interesting that curcumin, a phytochemical whose derivatives can be synthesized easily, have not been extensively studied for the SARS-CoV-2 virus. In light of this information, modifications to curcumin derivatives could provide an important research advance to increase the efficacy of current therapies used.

SARS-CoV-2 is an enveloped, positive sense, single-stranded RNA virus (Kim et al., 2020; Malone et al., 2022). The SARS-CoV-2 proteins consist of two large polyproteins named ORF1a and ORF1b (ORFs are proteolytically cleaved into 16 functional non-structural proteins (NSPs) (Rohaim et al., 2021)), four structural proteins (Envelope (E), Membrane (M), Nucleocapsid (N) spike (S) proteins)) and accessory proteins (Kim et al., 2020; Wu et al., 2020b). Most of these target proteins are considered as antiviral targets and the 3-D structure of almost all of them has been fully resolved and published in the protein data bank (PDB).

The group of non-structural proteins (NSPs) encoded by the viral genome consists of the NSP1, NSP2, NSP3 (Papain-like protease, PLpro), NSP4, NSP5 (main protease, 3CLpro), NSP6, NSP7/8/12(RNA-dependent RNA polymerase, RdRp), NSP9 (RNA replicase), NSP10/16 (2′O-Methyltransferase complex), NSP11, NSP13 (Helicase), NSP14 (N-terminal exoribonuclease, ExoN), NSP15 (Uridylate-specific endoribonuclease, NendoU) and NSP16 protein domains (Kim et al., 2020; Rohaim et al., 2021; Wu et al., 2020b). The main protease enzyme is also called chymotrypsin-like protease (3CLpro). The 3CLpro enzyme cleaves most of the NSP4–16 domains in polyproteins (Wu et al., 2020a) and the products are non-structural proteins (NSPs) that assemble into the replicase-transcriptase complex (RTC). On the other hand, papain-like cysteine protease (PLpro) cleaves NSP1–4 domains (Moustaqil et al., 2021). In other words, 3CLpro and PLpro work together to cleave polyproteins into NSPs, thereby they enhance coronaviral replication and lead viral spread (Harcourt et al., 2004; Lim et al., 2000). Therefore, it can be considered that 3CLpro and PLpro are the most important target protein structures for antiviral drugs. Another important target is NSP7/NSP8/NSP12 complex. Here, RNA-dependent RNA polymerase (RdRp) enzyme, also called NSP12, is involved in the replication and transcription of the SARS-CoV-2 genome (Wang et al., 2020) and bounds to its essential cofactors, NSP7 and NSP8. On the other hand, NSP15, one of the RNA-processing enzymes encoded by the coronavirus, (Posthuma et al., 2006) and NSP16, an RNA cap-modifying enzyme that is active only in the presence of its activating partner NSP10 (Rosas-Lemus et al., 2020), are also important drug target structures. In addition, as it is known, human angiotensin converting enzyme 2 (hACE2) is an enzyme bound to the membranes of cells in the heart, lungs, arteries, kidneys, and intestines (Donoghue et al., 2000; Hamming et al., 2004). The SARS-CoV-2 surface spike glycoprotein consists of three S1-S2 heterodimers. The receptor binding domain (RBD), located at the head of S1 and bound with the cellular receptor ACE2, initiates membrane fusion of virus and host cell (Hoffmann et al., 2020). During viral infection, ACE2 interacts with coronavirus spike proteins and allows the virus to enter the cell (Cao et al., 2020). Therefore, both S1 and ACE2 are considered as significant target structures for antiviral drugs.

In the light of these important literature data mentioned above, it was aimed to investigate the inhibition potentials of various curcumin derivatives on different target enzyme sites of SARS-CoV-2 in the presented study. As a result of in silico studies and analyses, it was observed that the curcumin derivatives proposed in this study had better ADME (absorption, distribution, metabolism, excretion) profiles and higher docking scores for all SARS-CoV-2 enzyme targets discussed in this paper than the reference drugs and enzyme inhibitors. Furthermore, it has been determined that curcumin derivatives have a higher affinity for the PLpro enzyme that the other SARS-CoV-2 target enzymes. To this end, molecular Dynamics (MD) simulations between curcumin derivatives with high docking score inhibitor/drug(ligand) and PLpro enzyme were performed and the binding stability of ligands to PLpro enzyme was evaluated using MM-PBSA (Molecular Mechanics Poisson-Boltzmann Surface Area) analysis. Moreover, PLpro residues that play a key role in binding have been identified. In conclusion, this study, which is the first step for drug design studies on target curcumin derivatives, is expected to be an important guidance for scientists who will conduct in vitro and in vivo studies.

2. Materials and methods

2.1. Design of curcumin derivatives

We based the main mentality of our work on curcumin derivatives being the interesting class of natural compounds with great pharmacological potentials. In this regard, it is thought that the activities of curcumin will increase even more by adding heterocyclic compounds such as 2 H-pyran-4 (3 H)-one and 1-methylpiperidin-4-one to these derivatives by (Bykhovskaya et al., 2017; Koroth et al., 2019; Murugesan et al., 2019; Roayapalley et al., 2021; Santiago-Vazquez et al., 2014). These compounds proposed in the study can be easily and quickly synthesized according to the synthesis method in the literature (Adams et al., 2004; Fawzy et al., 2015; Jha et al., 2006) (Scheme S1).

Also, the use of various electron-withdrawing (such as -F, -Cl, Br) (Nath et al., 2018; Roayapalley et al., 2021; Santiago-Vazquez et al., 2014) and donating groups (such as -OCH_3) (Badavath et al., 2016a, 2016b; Murugesan et al., 2019; Santiago-Vazquez et al., 2014) in the compounds can also cause significant changes in biological activities due to steric and electronic effects. To this end, we created a library containing 68 curcumin derivatives. We then eliminated these molecules according to their ADME profiles to put our study on a solid foundation. In this elimination, we used 5 different main drug filter approaches and accordingly, curcumin derivatives that violated the criteria of any of the 5 filter approaches by more than 1 were eliminated. It was finally identified 22 curcumin derivatives with a reliable ADME profile. In this context, Scheme 1 shows the designed various 2 H-pyran-4(3 H)-one and 1-methylpiperidin-4-one curcumin derivatives as target compounds. In addition, in this study, the ADME profiles of proposed 22 curcumin derivatives are scrutinized in detail, and investigated antiviral drug potencies against SARS-CoV-2 main enzymes by using molecular docking based virtual screening and MD simulations.

2.2. ADME and druglikeness parameters

ACD/ChemSketch was utilized for the 2D chemical drawing and editing in the SDF format for all compounds. Then, using these 2D structures, various in silico absorption, distribution, metabolism,

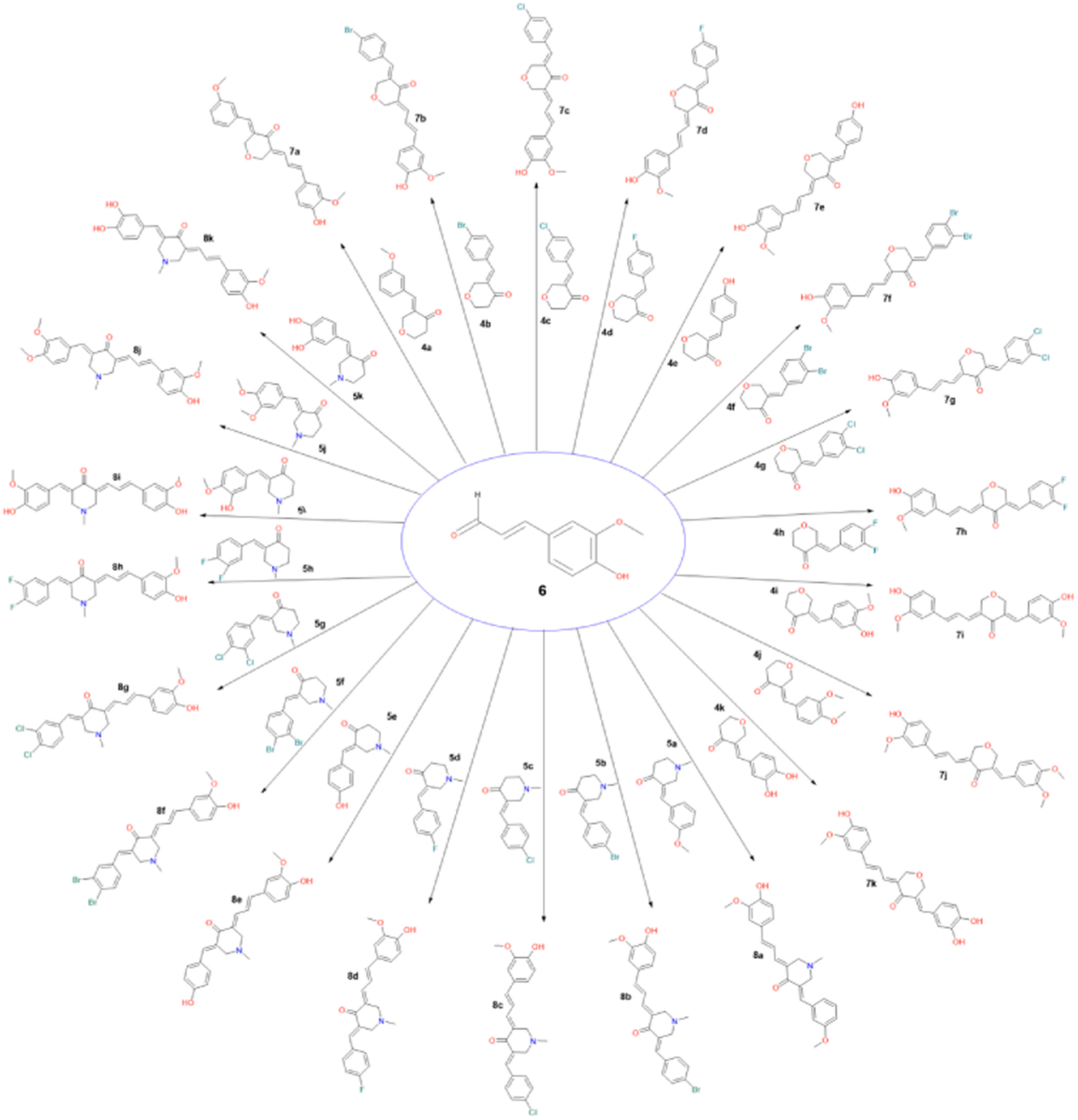

Scheme 1. The Representation of curcumin analogues and its 2 H-pyran-4(3 H)-one and 1-methylpiperidin-4-one derivatives.

excretion (ADME) and drug-likenesses properties of the compounds were investigated using the SwissADME webserver(Daina et al., 2014, 2017).

2.3. Molecular docking calculations

The docking simulations were performed using AutoDock Vina software (Trott and Olson, 2010) with the Lamarckian genetic algorithm (LGA) (Huey et al., 2007; Solis and Wets, 1981). Before the docking process, 2D structures of molecules prepared in SDF format were converted into 3D structures in MOL2 format using Open Babel, and then the energies of these 3D structures were minimized with the root mean square gradient (RMS 0.001 kcal/mol /A^2) using MMFF94 Forcefield parameters in Avogadro v.1.2.060 program (Hanwell et al., 2012). Then, these optimized compounds and target structures were prepared for docking using the PyRx program (Dallakyan and Olson, 2015). This program automatically removes all water molecules, ion, and etc. contents in PDB structures and added Kollman charges for the protein and Gasteiger charges for the ligand and cofactors.

In the docking studies, it was used target PDB ID's of the COVID-19 Docking Server (https://ncov.schanglab.org.cn/)(Kong et al., 2020). These relevant target PDB structures used in our study are generally the most preferred target structures in the literature. Similarly, for active binding pockets, Grid space values determined by the COVID-19

Docking Server were used. The grid space values of the COVID-19 Docking Server corresponds and includes to the active binding pockets of the reference inhibitors of each target enzyme. Also, in order to evaluate the accuracy of the grid space values of the COVID-19 Docking Server, we first performed blind docking studies for each target. Blind docking is the docking process of a ligand by scanning the whole surface of a protein without any prior knowledge of the target pocket. These trial blind docking studies showed that ligands majority bind to active binding pockets determined by the COVID-19 Docking Server, that is, active binding regions of reference ligands. Moreover, we selected exhaustiveness value as 32 in the all docking process to obtain a more consistent docking result.

In this study, docking simulations were conducted on 6 different SARS-CoV-2 target enzyme structures. The 3D conformational structures of these target proteins were obtained from the Research Collaboratory for Structural Bioinformatics (RCSB) Protein Database (http://www.rcsb.org/) (Berman et al., 2000). The PDB accession codes of the targets are 6LU7(Jin et al., 2020); 3CLpro with N3 inhibitor, 6WUU(Rut et al., 2020); PLpro with VIR250 inhibitor, 7BV2 (Yin et al., 2020); RdRp with triphosphate form of Remdesivir (F86), 6WLC (Kim et al., 2021); NSP15 with Uridine-5′-Monophosphate (U5p), 6WVN (Rosas-Lemus et al., 2020); NSP16 with 7-methyl-GpppA (GTA), S-Adenosylmethionine (SAM) and 7-methyl-guanosine-5′-triphosphate (MGP) inhibitors, 6M0J (Lan et al., 2020); The receptor binding domain (RBD) located on the head of Spike S1 subunit of the SARS-CoV-2 with hACE2. In docking simulations, the selected curcumin derivatives, inhibitors of the aforementioned receptors, and various references drugs (Favipiravir, Hydroxychloroquine, Lopinavir, Remdesivir, Warfarin (Coumadin)) that have been used and still used in the treatment of COVID-19 were taken as ligands.

Our molecular docking protocol was validated by superimposing the 3D binding pose of crystallized ligand (experimental inhibitor) and its docked binding pose and by computing their RMSD values. The superimposed configurations for reference inhibitors and their RMSD values were depicted in Fig. S1. This method is one of the most commonly used methods to determine the accuracy of a docking protocol. In this context, a docking method can be considered valid if the RMSD value between superimposed configurations of ligands is $\leq$ 2.0 Å (Abdusalam and Murugaiyah, 2020; Azam, 2021; C et al., 2022; Elhady et al., 2021). Accordingly, our results show that all reference inhibitors overlap almost perfectly with RMSD values obtained within these limits, therefore it can be said that our docking protocol is valid.

In addition, the docking values listed in the study for each ligand are their best binding affinity values against target enzymes, and similarly, the interaction diagrams belong to their relevant conformations with best binding energy.

2.4. Molecular dynamic simulation study and MM-PBSA calculations

MD simulations of the target protein (PLpro) and ligands (**8b**, **8c**, **8d**, **8f**, **8g**, **8h, 8k** curcumin derivatives, Remdesivir, VIR250) complexes were performed by GROMACS program version 2020.1 (Abraham et al., 2015). MD simulation was conducted for the timescale of 100 nano seconds (ns) using CHARMM36 (Huang and MacKerell Jr, 2013) force field and TIP3P(Jorgensen et al., 1983) water model were used for the protein and the explicit solvent, respectively. The CHARMM36 force field parameters for ligand were derived from CHARMM General Force Field (CGenFF) web server (Vanommeslaeghe et al., 2010; Yu et al., 2012).

In each MD simulation, the complexes were firstly centered in cubic box with dimensions 15 × 15 × 15 nm where the distance between the box and solutes was at least 1 nm. 44282 water molecules were subsequently added into the system. Then, a sufficient number of Na+ and Cl- to the system will be added to achieve system charge neutrality and a NaCl concentration of 0.150 M simultaneously.

Next, the energy of the prepared system was minimized for 4000 iteration steps by using the steepest descent method. Afterwards, the system was subjected to equilibration in two steps, each 1 ns, to stabilize both temperature and pressure of the system, respectively in NVT and NPT ensemble. Finally, the simulations of 100 ns for each complex system were performed in NPT ensemble. During the simulations, the temperature of 310 K were kept constant by a V-rescale algorithm ($\tau = 0.1$ ps)(Bussi et al., 2007) and pressure with Parinello–Rahman barostat ($\tau = 2.0$ ps)(Parrinello and Rahman, 1981) was 1 bar. LINCS algorithm(Hess, 2008) and Settle algorithm(Miyamoto and Kollman, 1992) were used to constraint the hydrogens and the solvent, respectively. The time step was set to 2 fs and data were saved every 20 ps to allow for detailed analysis with the tools available.

After the final production studies, RMSF (Root-Mean-Square-Fluctuation) analyses were performed to observe the effects of ligands on enzyme conformation and compared with the wild type form of the PLpro enzyme. After MD study, binding free energy was computed using Molecular mechanics Poisson-Boltzmann surface area (MM-PBSA) method (Kumari et al., 2014).

Binding free energy of the protein-ligand complex using MM-PBSA approximation can be calculated as follows:

$$\Delta E_{MMPBSA} = E_{complex} - (\quad E_{protein} + E_{ligand})$$

where $E_{complex}$ is the total MMPBSA energy of protein-ligand complex, $E_{protein}$ and E_{ligand} are the total free energies of the isolated protein and ligand, respectively. Each individual total free energy can (E_a) be expressed as:

$$E_a = E_{MM} + E_{solvation}$$

where E_{MM} is the sum of van der Waals energy (E_{vdW}) and electrostatic energy (E_{elec}) while $E_{solvation}$ contains polar (E_{polar}) and nonpolar ($E_{non\text{-}polar}$) solvation energy contributions.

3. Results and discussion

3.1. Predictions of ADME and drug-likeness parameters

The ADME properties of the compounds allow drug developers to understand the reliable and efficacy of a drug candidate compound and thus, they accelerate the timeline for new drug submission process to the FDA. Therefore, inadequate evaluation of the ADME parameters and drug-like nature of novel compounds proposed as drug candidates causes many biologically active compounds to fail before they reach the clinic. To this end, we first evaluated the ADME parameters of the proposed curcumin derivatives and their similarities to existing drugs in order to put our study on a firm basis. For this purpose, in the presented study, we focused on curcumin derivatives that comply with a set of rules based on ADME parameters applied by various drug filters and are therefore likely to be drug candidates. Here, the similarities of new drug candidate compounds to available drugs were evaluated by considering the rules of five different filter approaches applied by major drug developers around the world. The five different drug filter approaches in our study and the criteria they apply are as follows.

- Lipinski (Pfizer) filter (Lipinski et al., 1997): MW$\leq$ 500; MLOGP $\leq$ 4.15; HBA$\leq$ 10; HBD$\leq$ 5
- Ghose filter (Ghose et al., 1999): 160 $\leq$MW$\leq$ 480; $-$ 0.4 $\leq$WLOGP $\leq$ 5.6; 40 $\leq$MR$\leq$ 130; 20 $\leq$atoms$\leq$ 70
- Veber (GSK) filter (Veber et al., 2002): RB$\leq$ 10; TPSA$\leq$ 140
- Egan (Pharmacia) filter (Egan et al., 2000): WLOGP$\leq$ 5.88; TPSA$\leq$ 131.6
- Muegge (Bayer) filter (Muegge et al., 2001): 200 $\leq$MW$\leq$ 600, $-$ 2 $\leq$XLOGP$\leq$ 5; TPSA$\leq$ 157; HBA$\leq$ 10; HBD$\leq$ 5; RB $\leq$ 15; Number of rings$\leq$ 7; Number of carbons$>$ 4; Number of heteroatoms$>$ 1

Table 1 shows the ADME parameters related to the physicochemical

Table 1
Various ADME parameters for all compounds.

Compounds	Physicochemical Properties								Lipophilicity					
	MW (g/mol)	heavy atoms	aromatic heavy atoms	RB	HBA	HBD	MR	tPSA (Å^{2})	ilogP	XlogP	WlogP	MlogP	SILICOS-IT	Consensus logP
7a	378.42	28	12	5	5	1	108.69	64.99	3.83	3.68	3.81	2.06	4.99	3.67
7b	427.29	27	12	4	4	1	109.90	55.76	3.94	4.40	4.57	3.00	5.60	4.30
7c	382.84	27	12	4	4	1	107.21	55.76	3.86	4.34	4.46	2.89	5.56	4.22
7d	366.38	27	12	4	5	1	102.16	55.76	3.70	3.81	4.36	2.78	5.34	4.00
7e	364.39	27	12	4	5	2	104.22	75.99	3.28	3.35	3.51	1.85	4.44	3.28
7f	506.18	28	12	4	4	1	117.60	55.76	4.22	5.09	5.33	3.58	6.28	4.90
7g	417.28	28	12	4	4	1	112.22	55.76	4.04	4.96	5.11	3.37	6.20	4.74
7h	384.37	28	12	4	6	1	102.11	55.76	3.74	3.91	4.92	3.16	5.76	4.30
7i	394.42	29	12	5	6	2	110.71	85.22	3.74	3.32	3.52	1.52	4.51	3.32
7j	408.44	30	12	6	6	1	115.18	74.22	3.96	3.65	3.82	1.73	5.06	3.64
7k	380.39	28	12	4	6	3	106.24	96.22	3.12	3.00	3.22	1.30	3.96	2.92
8a	391.46	29	12	5	5	1	119.22	59.00	4.08	3.86	3.35	2.27	4.62	3.64
8b	440.33	28	12	4	4	1	120.43	49.77	4.24	4.58	4.10	3.21	5.23	4.27
8c	395.88	28	12	4	4	1	117.74	49.77	4.19	4.52	3.99	3.10	5.19	4.20
8d	379.42	28	12	4	5	1	112.69	49.77	4.02	3.99	3.90	3.00	4.97	3.98
8e	377.43	28	12	4	5	2	114.75	70.00	3.54	3.54	3.05	2.06	4.07	3.25
8f	519.23	29	12	4	4	1	128.13	49.77	4.10	5.28	4.86	3.78	5.91	4.79
8g	430.32	29	12	4	4	1	122.75	49.77	4.24	5.15	4.65	3.58	5.84	4.69
8h	397.41	29	12	4	6	1	112.65	49.77	3.62	4.09	4.46	3.37	5.40	4.19
8i	407.46	30	11	5	6	2	121.25	79.23	4.11	3.51	3.05	1.73	4.15	3.31
8j	421.49	31	12	6	6	1	125.72	68.23	3.82	3.84	3.36	1.93	4.70	3.53
8k	353.43	29	12	4	6	3	116.78	90.23	3.40	3.18	2.75	1.52	3.60	2.89
Bisdemethoxycurcumin	308.33	23	12	6	4	2	89.82	74.60	1.75	3.26	3.13	2.13	3.87	2.83
Curcumin	368.38	27	12	8	6	2	102.80	93.06	3.27	3.20	3.15	1.47	4.04	3.03
Demethoxycurcumin	338.35	25	12	7	5	2	96.31	83.83	2.78	3.32	3.14	1.80	3.95	3.00
F86	371.24	25	9	4	10	5	79.39	206.26	-0.30	-3.06	-1.84	-2.57	-3.09	-2.17
Favipiravir	157.10	11	6	1	4	2	32.91	88.84	0.39	-0.56	-0.57	-1.30	0.69	-0.27
GTA	787.44	51	18	12	21	10	163.35	427.83	-4.84	-7.90	-4.47	-5.16	-8.27	-6.17
Hydroxychloroquine	335.87	23	10	9	3	2	98.57	48.39	3.58	3.58	3.59	2.35	3.73	3.37
Lopinavir	628.80	46	18	17	5	4	187.92	120.00	3.84	5.92	3.57	2.93	6.02	4.45
MGP	538.21	33	9	8	15	8	104.03	319.52	-5.35	-5.60	-3.22	-4.08	-5.86	-4.82
N3	680.79	49	11	22	9	5	184.13	197.83	3.73	3.35	1.55	0.38	4.42	2.69
Remdesivir	602.58	42	15	14	12	4	150.43	213.36	2.77	1.91	2.21	0.18	-0.05	1.41
SAM	398.44	27	9	7	9	4	96.51	210.76	0.00	-3.49	-3.57	-3.97	-3.37	-2.88
U5p	324.18	21	6	4	9	5	65.18	181.12	-0.40	-3.63	-3.06	-2.60	-2.52	-2.44
Warfarin	308.33	23	16	4	4	1	88.58	67.51	2.41	2.70	3.61	2.51	4.36	3.12
VIR250	520.60	36	9	19	8	5	132.69	209.85	2.30	-0.31	-0.64	-1.24	2.48	0.52

and lipophilic properties of the proposed compounds and reference enzyme inhibitors and drugs. The physicochemical parameters calculated in the study included the molecular weight (MW), the number of heavy atoms, rotatable bond count, various hydrogen bond properties, molecular refractivity (MR), and topological polar surface area (tPSA). Among these, the MR value is defined as a measure of the overall polarity of a compound, and this parameter, used by the Ghose filter (Ghose et al., 1999), is generally suggested to be in the range of 40–130. Examining MR values in the table, all the proposed drug candidate curcumin derivatives are within this recommended value range, but the MR values of some reference drugs and inhibitors (GTA (163.35), Lopinavir (187.92), Remdesivir (150.43) and N3(184.13)) used in the study are higher than the recommended value range. tPSA values, on the other hand, are the sum of the surface areas of polar atoms in a molecule and are a parameter related to the drug carrying capacity of a compound. According to the table, it is observed that the values obtained for the drug candidate curcumin derivatives meet the criteria applied for the tPSA values of the drug filter approaches used in the study ($\leq$131.6 for Egan (Egan et al., 2000), $\leq$ 140 for Veber (Veber et al., 2002), $\leq$ 157 for Muegge (Muegge et al., 2001)). Also, all reference drugs and inhibitors except F86, Favipiravir, Hydroxychloroquine and Warfarin were seen to violate the tPSA criterion of at least one drug filter approach.

Furthermore, **7f** (506.18 g/mol) and **8f** (519.23 g/mol) compounds containing 3,4-dibromo substituents, among the proposed curcumin derivatives, slightly exceed the upper limit values of the MW criteria determined by both Lipinksi and Ghose filters (MW$\leq$500 for Lipinkski, 160 $\leq$MW$\leq$480 for Ghose, 200 $\leq$MW$\leq$600 for Muegge). As it is seen in the table, all curcumin derivatives other than these meet the MW criteria of drug filters. On the other hand, reference inhibitors and drugs except F86, Hydroxychloroquine, SAM, U5p and Warfarin violate the MW criteria of at least one filter approach. In addition, for other physicochemical parameters, it can be said that the proposed curcumin derivatives meet the criteria of filter approaches whereas there are some violations for reference drugs and inhibitors.

The lipophilicity parameters in the table express the solubility of a chemical compound in fats, lipids, and non-polar solvents such as hexane or toluene and are hence a valuable parameter influencing the activity of the drug in the human body. LogP values are the most widely used measure of lipophilicity and are an indicator of the permeability of drugs to reach target tissue in the body. In this regard, the LogP values used by the various drug filters and their mean values (consensus logP) are represented in Table 1.

Table 2 lists the parameters violated for criteria of the aforementioned drug filter approaches for each compound. When the curcumin derivatives proposed in this study are compared among themselves, it is seen that the **7f** and **8f** compounds containing 3,4-dibromo substituents violate the threshold values applied for the MW values of the Lipinski and Ghose filters and for the lipophilicity values of Muegge. Similarly, it is observed that **8g** compound containing 3,4-dichloro group as substituent only violates the criteria applied by Muegge filter for lipophilicity. Apart from these violations, it seems that the proposed curcumin derivatives do not violate the rules of any drug filter approach. On the other hand, drug filter approaches generally state that an orally active drug should not violate its own criteria more than once (Benet et al., 2016; Bickerton et al., 2012; Lipinski et al., 2001; Petit et al.,

Table 2
Violation of drug-likeness filters for all compounds.

Compounds	Lipinski	Ghose	Veber	Egan	Muegge
7a	0	0	0	0	0
7b	0	0	0	0	0
7c	0	0	0	0	0
7d	0	0	0	0	0
7e	0	0	0	0	0
7f	MW> 500	MW> 480	0	0	XLOGP3 > 5
7g	0	0	0	0	0
7h	0	0	0	0	0
7i	0	0	0	0	0
7j	0	0	0	0	0
7k	0	0	0	0	0
8a	0	0	0	0	0
8b	0	0	0	0	0
8c	0	0	0	0	0
8d	0	0	0	0	0
8e	0	0	0	0	0
8f	MW> 500	MW> 480	0	0	XLOGP3 > 5
8g	0	0	0	0	XLOGP3 > 5
8h	0	0	0	0	0
8i	0	0	0	0	0
8j	0	0	0	0	0
8k	0	0	0	0	0
bisdemethoxycurcumin	0	0	0	0	0
curcumin	0	0	0	0	0
demethoxycurcumin	0	0	0	0	0
F86	NorO> 10	WLOGP< −0.4	TPSA> 140	TPSA> 131.6	XLOGP3 < −2 TPSA> 150
Favipiravir	0	MW< 160 WLOGP< −0.4 MR< 40 #atoms< 20	0	0	MW< 200
GTA	MW> 500 NorO> 10 NHorOH> 5	MW> 480, WLOGP< −0.4 MR> 130 #atoms> 70	Rotors> 10 TPSA> 140	TPSA> 131.6	MW> 600 XLOGP3 < −2 TPSA> 150 H-acc> 10 H-don> 5
Hydroxychloroquine	0	0	0	0	0
Lopinavir	MW> 500	MW> 480 MR> 130 #atoms> 70	Rotors> 10	0	MW> 600 XLOGP3 > 5 Rotors> 15
MGP	MW> 500 NorO> 10 NHorOH> 5	MW> 480, WLOGP< −0.4	TPSA> 140	TPSA> 131.6	XLOGP3 < −2 TPSA> 150 H-acc> 10 H-don> 5
N3	MW> 500 NorO> 10	MW> 480 MR> 130 #atoms> 70	Rotors> 10, TPSA> 140	TPSA> 131.6	MW> 600 TPSA> 150 Rotors> 15
Remdesivir	MW> 500 NorO> 10	MW> 480 MR> 130 #atoms> 70	Rotors> 10 TPSA> 140	TPSA> 131.6	MW> 600 TPSA> 150 H-acc> 10
SAM	NorO> 10	WLOGP< −0.4	TPSA> 140	TPSA> 131.6	XLOGP3 < −2 TPSA> 15
U5p	NorO> 10	WLOGP< −0.4	TPSA> 140	TPSA> 131.6	XLOGP3 < −2 TPSA> 15
Warfarin	0	0	0	0	0
VIR250	MW> 500 NorO> 10	MW> 480 WLOGP< −0.4 MR> 130	Rotors> 10 TPSA> 140	TPSA> 131.6	TPSA> 150 Rotors> 15

2012; Shen et al., 2012; Sreelakshmi et al., 2017). Accordingly, it can be stated that all of the proposed curcumin derivatives meet the criteria of the five different main drug filter approaches discussed in the paper. In addition, three natural curcuminoids, which are in the GRAS class by the FDA, obey all the rules of drug filter approaches. This supports the reasons why we prefer curcumin derivatives in our study.

When the violations of the drug filter approaches of reference drugs and inhibitors are scrutinized, it is seen that Hydroxychloroquine and Warfarin meet all the criteria of the main five filter approach, while other reference drugs and inhibitors violate at least two drug filter approach once or more than once. The ADME properties examined in this study so far are sufficient to indicate that natural curcuminoids and 22 proposed curcumin derivatives have much better and safer ADME parameters than the vast majority of reference inhibitors and drugs.

Brain access and gastrointestinal absorption are two decisive criteria for predicting pharmacokinetic behaviour at various stages of the drug discovery processes. For this purpose, the Brain or IntestinaL EstimateD permeation method (BOILED-Egg) is suggested as a prediction model based on the polarity parameters (tPSA) and lipophilicity (WlogP) of molecules.

The BOILED-Egg map obtained from the Swiss-ADME web server for compounds was depicted in Fig. 1. On the map, the white elliptical region is the physicochemical area of molecules that have a high probability of being absorbed by the gastrointestinal tract, while the yellow elliptical region corresponds to the physicochemical area of molecules with both high brain penetration and high gastrointestinal absorption probability. Reference inhibitors GTA, MGP, are completely out of this map. It is also seen that reference inhibitors N3, F86, U5p, SAM, VIR250

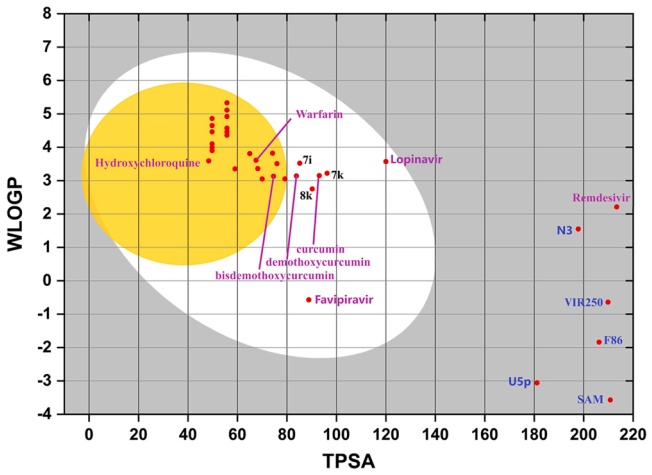

Fig. 1. The map of BOILED-Egg for all compounds. Here, the yellow region (yolk) is the physicochemical area of molecules most likely to penetrate the brain while the white area corresponds to the physicochemical area of molecules most likely to be absorbed by the gastrointestinal tract. Yolk and white areas in the map are not mutually exclusive. Here, reference drugs were written in purple text, while blue was used for reference inhibitors.

and reference drug Remdesivir are quite outside of both the white and yellow ellipse regions. Reference drug Lopinavir, Favipiravir, **7i**, **8k**, **7k** curcumin derivatives, natural curcumin and demethoxycurcumin are in the white zone. It is, herein, noteworthy point that vast (19 of 22 pieces) of the proposed curcumin derivatives, together with warfarin and Hydroxychloroquine, are located in the yellow region.

According to the BOILED-Egg analysis, it was determined that the majority of the proposed curcumin derivatives are compounds with both high brain penetration and high gastrointestinal absorption probability. In summary, it is clear that curcumin derivatives have significantly better pharmacokinetic behaviours than reference drugs and enzyme inhibitors.

In addition to the ADME parameters investigated so far, we have calculated different parameters for natural curcuminoids using the traditional Chinese medicine systems pharmacology database and analysis platform (TCMSP web-server) (Ru et al., 2014) and listed in Table 3. Here, our aim is to observe the correlation between the parameters we have calculated so far and the values calculated by the TCMSP server, and to get predictions for the suggested curcumin analogues about different parameters computed by TCMSP server. Fractional water accessible surface area of all atoms with negative partial charge (FASA-) is a drug-likeness parameters and Shen et al. (2012) reported that the compounds in the Traditional Chinese Medicine Compound Database can be a good source of drug-like molecules. Accordingly, the presence of curcuminoids in this library may indicate the importance of curcumin derivatives. DL (Drug-likeness), another drug similarity parameter, is a qualitative parameter that helps optimize pharmaceutical and pharmacokinetic properties of compounds such as chemical stability and solubility. The "DL" level used as a selection criterion for compounds in traditional Chinese herbs is $\geq$ 0.18 (Tao et al., 2013) and as it seen, curcuminiods meet these criteria. In TCMSP, Caco-2 is a parameter indicating epithelial permeability, while OB (Oral bioavailability) represents the percentage of orally administered drug that reaches the systemic circulation unchanged (Xu et al., 2012). On the other hand, In the SwissADME webserver, the Abbott bioavailability score is a parameter that tries to predict the measurable Caco-2 permeability of a compound and the probability of having at least 10% oral bioavailability in the rat. furthermore, this percentage score based on the total charge, the TPSA and the violation of the Lipinski filter of the compound defines four classes of compounds with probabilities of 11%, 17%, 56% or 85%. Accordingly, it was found to have a bioavailability score of 56% for natural curcuminoids, indicating that natural curcuminoids have good bioavailability. BBB (blood-brain barrier) in TCMSP web-server is a parameter used to understand and evaluate the capacity of compounds to enter the central nervous system. According to TCMSP, compounds with a BBB < -0.3 are defined as non-penetrating (BBB-) compounds (Tattersall et al., 1975). The map of BOILED-Egg in the SwissADME web server approximately corresponds to BBB parameter in TCMSP. In the map, natural curcuminoids are located in the white area in this map, which show that they can pass through the gastrointestinal tract well, but that it is less absorbed from the brain barriers. These findings almost coincide with the TMSP web server findings. On the other hand, the map predicts that the vast majority of proposed curcumin derivatives can pass through the brain barrier. the inference indicate that the proposed curcumin derivatives may have better pharmaceutical properties than natural curcuminoids.

3.2. Molecular docking studies

Molecular docking simulations were performed to determine the binding affinities between the 22 proposed curcumin derivatives and the target SARS-CoV-2 enzyme sites and to identify the molecular interactions that play a key role in binding. In order to compare the obtained values for curcumin derivatives, docking analyses were also conducted for natural curcuminoids, own inhibitors of each SARS-CoV-2 target enzyme structure, and various reference drugs whose effectiveness against COVID-19 was determined. The all values obtained as a result of the calculations are presented in Table 3.

When the docking scores of the curcumin derivatives containing the 2 H-pyran-4(3 H)-one group (**7a-7k**) and the 1-methylpiperidin-4-one group (**8a-8k**) are compared among themselves, the **8a-8k** compounds are generally observed to have slightly higher docking affinity values than **7a-7k** compounds ones (except Spike and Spike+ACE). Also, it is seen that the affinity values for the PLpro protein enzyme target of the proposed curcumin derivatives are higher than the other target enzyme regions. This situation indicates that the proposed curcumin compounds may have a significant and strong inhibitory effect, especially on the PLpro protein enzyme. In order to be better understood the above-mentioned inferences, we calculated the average binding energy values for each series of compounds and the obtained values were depicted as a bar graph in Fig. 2.

Furthermore, when the obtained docking scores are compared, it is understood that the proposed curcumin derivatives are significantly more effective on SAR-COV2 target structures than natural curcuminoids. This indicates the importance of focusing on various derivatives of natural phytochemicals to provide research progress in their current therapeutic applications.

When the docking affinity values obtained for each target protein enzyme structure in Table 4 are evaluated separately, it is seen for 3CLpro (main protease) target structure that the highest values binding affinity was obtained for **7h** (−8.3 kcal/mol) and **8h** (−8.4 kcal/mol) compounds. It is also observed that the affinity values of **7h** and **8h**

Table 3
Various ADME parameters for natural curcuminoids obtained from TCMSP.

Molecule ID	Molecule name	MW	HBD	HBA	RB	tPSA	Caco-2	BBB	DL	FASA-	OB
MOL002581	Curcumin	368.41	2	6	8	93.06	0.32	-0.60	0.41	0.34	4.37
MOL001603	Demethoxycurcumin	338.38	2	5	7	83.83	0.34	-0.59	0.33	0.41	4.37
MOL000945	Bisdemethoxycurcumin	308.35	2	4	6	74.60	0.35	-0.48	0.26	0.46	3.55

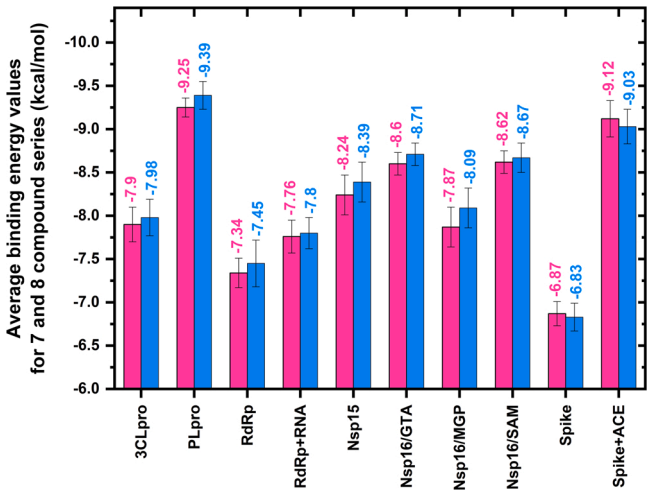

Fig. 2. Average binding energies of 7 and 8 compound series against the target SARS-CoV-2 enzymes. Here, compound 7 series was presented with pink bars while compound 8 series was represented with blue bars.

compounds are even higher than the main protease enzyme inhibitor N3 (−8.0 kcal/mol) molecule and Remdesivir (−8.1 kcal/mol), which is the drug with the highest affinity for this target.

On the other hand, the docking scores obtained for the RdRp+RNA target structure are higher than the affinity values obtained in docking simulations using the alone RdRp target. Almost all of the proposed curcumin derivatives were also observed to have higher affinity values than both the reference drugs and the F86 molecule, the inhibitor of RdRp. The remarkable point here is that, as in the main protease target region, the highest affinity value for the RdRp+RNA complex was obtained for **8h** compound (−8.1 kcal/mol).

For the NSP15 target region, the proposed curcumin derivatives have higher binding affinity than the reference drugs Favipiravir, Hydroxychloroquine, Remdesivir and Warfarin. It has been determined that although Lopinavir (−8.1 kcal/mol), one of the reference drugs, has a very good affinity on the NSP15 target site, it has a lower value than most of the proposed curcumin derivatives. On the other hand, U5p (−6.6 kcal/mol), inhibitor of the target enzyme, has a very low value. Among the proposed curcumin derivatives, the compound with the highest affinity is **8h** (−8.7 kcal/mol), as in the main protease and RdRp+RNA complex enzyme targets.

For the NSP16 enzyme, three different inhibitors (GTA, MGP, SAM) have been reported for three different active binding sites in the literature, therefore, the active binding regions on NSP16 enzyme of GTA, MGP, SAM molecules have been conducted separately in docking simulations. When the values obtained for three different NSP16 binding sites are probed in the table, it is seen that the proposed curcumin derivatives show higher affinity for the NSP16/GTA, NSP16/SAM active binding sites than the NSP16/MGP one. The **8f** and **8g** (−8.9 kcal/mol) compounds have the highest binding energy values for both NSP16/GTA and NSP16/SAM active binding sites while for NSP16/MGP active binding site, **8h** (−8.5 kcal/mol) is compound with the highest affinity value. The remarkable point here is that the GTA inhibitor has significantly a high binding affinity (−10.4 kcal/mol) at its binding site. On the other hand, self-inhibitors of other NSP16 active binding sites (SAM and MGP) and reference drugs have lower affinity values than the

Table 4
The obtained docking scores (kcal/mol) against various SARS-COV-2 target structures of all compounds.

Compounds	3CLpro	PLpro	RdRp	RdRp +RNA	Nsp15	Nsp16 /GTA	Nsp16 /MGP	Nsp16 /SAM	Spike	Spike +ACE
7a	-7.9	-9.3	-7.5	-7.6	-8.1	-8.6	-7.8	-8.6	-6.9	-9.0
7b	-7.9	-9.3	-7.2	-7.6	-8.4	-8.5	-7.6	-8.6	-7.0	-9.2
7c	-7.9	-9.3	-7.2	-7.7	-8.4	-8.5	-8.0	-8.6	-6.9	-9.1
7d	-8.0	-9.3	-7.3	-7.9	-8.4	-8.5	-8.1	-8.5	-6.9	-9.2
7e	-7.7	-9.2	-7.2	-7.8	-8.2	-8.4	-7.7	-8.4	-6.7	-8.9
7f	-8.0	-9.4	-7.4	-7.6	-8.4	-8.8	-7.9	-8.8	-7.1	-9.4
7g	-8.0	-9.3	-7.4	-8.0	-8.4	-8.7	-8.1	-8.8	-6.8	-9.4
7h	-8.3	-9.3	-7.6	-8.0	-8.5	-8.8	-8.3	-8.7	-6.8	-9.4
7i	-7.8	-9.2	-7.5	-7.7	-7.9	-8.6	-7.7	-8.6	-7.0	-8.9
7j	-7.5	-9.0	-7.0	-7.5	-7.8	-8.7	-7.6	-8.7	-6.6	-8.9
7k	-7.9	-9.1	-7.4	-8.0	-8.1	-8.5	-7.8	-8.5	-6.9	-8.9
8a	-7.8	-9.2	-7.5	-7.6	-8.2	-8.7	-8.0	-8.7	-6.7	-9.0
8b	-8.0	-9.4	-7.2	-7.6	-8.6	-8.6	-8.0	-8.5	-6.7	-9.3
8c	-8.0	-9.4	-7.2	-8.0	-8.6	-8.6	-8.2	-8.6	-6.6	-9.2
8d	-8.0	-9.5	-7.5	-8.0	-8.6	-8.7	-8.4	-8.6	-6.7	-9.1
8e	-7.8	-9.4	-7.3	-7.8	-8.3	-8.5	-8.0	-8.4	-6.8	-8.9
8f	-8.1	-9.5	-7.6	-7.8	-8.5	-8.9	-8.0	-8.9	-6.8	-8.8
8g	-8.1	-9.6	-7.4	-7.8	-8.6	-8.9	-8.3	-8.9	-7.0	-8.9
8h	-8.4	-9.6	-7.6	-8.1	-8.6	-8.8	-8.5	-8.8	-7.0	-9.4
8i	-7.9	-9.1	-7.9	-7.8	-8.1	-8.7	-7.9	-8.7	-6.9	-8.9
8j	-7.6	-9.2	-7.0	-7.5	-8.0	-8.8	-7.7	-8.8	-6.8	-8.9
8k	-8.1	-9.4	-7.8	-7.8	-8.2	-8.6	-8.0	-8.5	-7.1	-8.9
bisdemethoxycurcumin	-7.3	-7.5	-6.7	-7.2	-7.4	-8.1	-7.1	-7.3	-6.4	-7.7
curcumin	-7.3	-8.0	-7.2	-6.3	-7.2	-7.6	-7.1	-8.2	-7.1	-8.1
demethoxycurcumin	-7.4	-7.9	-6.8	-7.1	-7.4	-7.7	-7.2	-7.5	-6.6	-8.2
Favipiravir	-5.6	-5.7	-6.3	-5.2	-5.0	-6.1	-4.9	-6.0	-5.4	-6.6
Hydroxychloroquine	-6.4	-6.7	-5.2	-5.9	-6.1	-6.6	-6.0	-6.3	-4.9	-6.1
Remdesivir	-8.1	-8.8	-7.9	-7.6	-7.6	-8.0	-7.0	-8.4	-7.0	-8.0
Warfarin(coumadin)	-6.9	-8.0	-7.3	-6.7	-7.6	-7.7	-6.8	-7.7	-6.7	-7.7
Lopinavir	-7.9	-8.7	-7.4	-7.2	-8.1	-7.9	-7.5	-8.1	-6.8	-7.6
N3	-8.0									
VIR250		-7.6								
F86			-6.9	-6.6						
U5p					-6.6					
GTA						-10.4				
MGP							-6.5			
SAM								-7.4		
Kobophenol A									-8.9	-9.8

proposed curcumin derivatives. Also, it can be concluded according to the value trend of docking score that proposed curcumin derivatives can have a more inhibition effect on the NSP16 enzyme than the 3CLpro and RdRp target enzymes.

Another target structure in the study is Spike protein, and docking simulations were also performed using both alone Spike and Spike+ACE complex targets. When trend of docking score for these targets is examined in the Table 3, it is seen that docking values obtained for the Spike+ACE complex are the higher than values obtained for alone Spike region is targeted. According to the docking results obtained using alone Spike enzyme as a target, it was observed that the natural curcumin, **8f** and **8g** compounds has the highest affinity values with − 8.1 kcal/mol. Here, it is noteworthy that natural curcumin is among the compounds with the highest affinity for docking simulations used alone Spike protein as target. For natural curcumin, this case is unique among docking studies on 10 different target SARS-CoV-2 targets. On the other hand, the highest affinity values for Spike+ACE complex were obtained for compounds **7f**, **7g**, **7h** and **8h** with − 9.4 kcal/mol. Here, Kobophenol A, first natural inhibitor, appears as the compound with the highest docking score for these target structures. Gangadevi et al. (2021) reported that Kobophenol A inhibited ACE2 binding to SARS-CoV-2 S1-RBD in vitro with an IC50 of 1.81 ± 0.04 μM. According to docking findings in the same study, it was found that Kobophenol A bound to the ACE2/spike interface with − 11.15 kcal/mol while Curcumin bound with − 8.42 kcal/mol. Accordingly, these results are in good coherence with our findings.

Finally, when the docking scores obtained for the PLpro target, which has the highest value trend for curcumin derivatives among all target regions, are scrutinized in detail, the 22 proposed curcumin derivatives are significantly higher affinity values than all other reference drugs, PLpro enzyme inhibitor VIR250 (−7.6 kcal/mol) of and natural curcuminoids. Here, although the binding affinity values obtained for the curcumin derivatives are quite close to each other, the highest values were obtained for **8g** and **8h** compounds (−9.6 kcal/mol), followed by **8d** and **8f** compounds (−9.5 kcal/mol). Following these, some curcumin derivatives with the highest values are **8b**, **8c** and **8k**. When all these findings for PLpro are evaluated together, it is seen that the all of high-affinity curcumin derivatives **8b**, **8c, 8d**, **8f**, **8g, 8h** and **8k** have in the 1-methylpiperidin-4-one group and include 4-bromo, 4-chloro, 4-fluoro, 3,4-dibromo, 3,4-dichloro, 3,4-difluoro and 3,4-hydroxyl substituents of this group. These inferences may be key insights in future compound designs with high affinity. Hence, it is expected that these findings obtained as a result of the analyses will be a guide for other working groups that will design inhibitors for the PLpro enzyme in the future.

In addition, it has been reported that inhibitor N3 in the first X-ray structure published (PDB ID:6LU7) for the main protease (3CLpro) exhibited inhibition against SARS-CoV-2 with individual half-maximum effective concentration (EC50) values of 16.77 μM (Jin et al., 2020). On the other hand, it was not reported experimental value such as IC50 or EC50 for VIR250, the inhibitor of the first reported x-ray structure (PDB ID: 6WUU) for PLpro, however it can be estimated from the inhibition curve that the IC 50 for VIR250 is around 10 μM (Rut et al., 2020). When the docking scores obtained for N3 against the 3CLpro and VIR250 against PLpro target structure are compared with the docking scores obtained for the proposed curcumin derivatives, it reveals an important prediction about the high inhibition potentials of the proposed curcumin derivatives for 3CLpro, PLpro and other SARS-CoV-2 target enzymes.

In addition, we displayed 2D molecular interaction diagrams between the dimeric PLpro target enzyme and all compounds (Fig. S2-S32). From the diagrams, the types of molecular interactions, the interacting atoms of the compounds and the interacting residues of the dimeric PLpro chains can be clearly seen.

Comparing the highest binding affinity curcumin derivatives **8b, 8c, 8d, 8f, 8g, 8h and 8k** for PLpro with the PLpro enzyme inhibitor VIR250 and the reference drug Remdesivir reference drug can be a good method for in-depth inferences. In this regard, in order to be easier and clearer understanding, we also listed the interacting residues of the dimeric PLpro enzyme with the relevant compounds mentioned above, molecular interaction types and their properties in Table 5.

According to the table, it is observed that compounds **8d** and **8h** form a halogen type interaction with PLpro enzyme via 4-fluorine and 3,4-difluorine substituents, on the other hand **8b, 8c, 8f** and **8g** compounds, form alkyl type hydrophobic interaction with PLpro enzyme via their 4-bromo, 3-chloro 3,4-dibromo and 3,4-dichloro substituents. Also, it is remarkable that **8k** compound form conventional hydrogen bond with PLpro enzyme via their 4-hydroxyl substituents. In this regard, these interactions between the substituents of **8b, 8c, 8d, 8f, 8g, 8h and 8k** compounds and the PLpro enzyme may be the main reason that allows them to have higher docking scores compared to other curcumin derivatives.

When the hydrogen bond interactions, which are a significant factor for a compound to be a drug, are scrutinized, it is seen that all of **8b, 8d**, **8f**, **8g** and **8h** curcumin derivatives form carbon hydrogen bonds with the Pro248 residue of PLpro. Hence it can be considered that Pro248 has a key role in the binding of curcumin derivatives to PLpro enzyme. Moreover, it is striking point that both **8d** and **8h** compounds containing 4-fluorine and 3,4-difluorine substituents, respectively, have 4 hydrogen bond interactions with PLpro while **8b** and **8k** compound containing 4-bromo and 3,4-hydroxy substituents, respectively, have 3 hydrogen bond interactions with PLpro. On the other hand, each of **8f** and **8g** compounds containing 3,4-dibromo and 3,4-dichloro substituents, respectively, have only 1 hydrogen bond interaction. While the reference drug Remdesivir has 4 conventional hydrogen bonds, on the other hand, the fact that the PLpro inhibitor VIR250 has 9 Hydrogen bond interactions and 5 of them are with the Arg166 residue of the PLpro enzyme can be very critical for this inhibitor. Here, although VIR250 has such a large number of hydrogen bond interactions, the low binding affinity of VIR250 can be attributed to the relatively lower electrostatic and hydrophobic interactions of VIR250 compared to other compounds. It can be also said that another reason for the low affinity of VIR250 is the unfavourable interaction of VIR250 with the Arg106 residue of PLpro. Similarly, although the reference drug Remdesivir has very high hydrophobic and 4 hydrogen bond interactions, it has lower binding affinity than curcumin derivatives such as VIR250. As it can be clearly understood from the table, the reason for this situation can be considered as 3 unfavourable interactions of Remdesivir with the Arg166 residue of PLpro. In the light of the findings obtained so far, it can be inferred that the curcumin derivatives have no unfavourable interactions with PLpro compared to reference drugs and hence this highlights curcumin derivatives for high docking scores.

For the electrostatic interactions according to the table, it can be said that the Glu161 and Asp164 residues of PLpro have very critical roles. On the other hand, examining the hydrophobic interactions, it is observed that there are common hydrophobic interactions between all of the curcumin derivatives discussed and the Tyr264, Tyr207, Pro248 residues of the PLpro enzyme. This indicates that these residues play a key role in the hydrophobic interactions between curcumin derivatives and the PLpro enzyme.

Moreover, in order to better envision the active binding sites on the PLpro enzyme conformation of the above-mentioned compounds, their binding sites on PLpro are displayed in Fig. 3. The PLpro chain discussed in the study has two homo anti-parallel chains named Chain A and C, in other words, it is in a dimeric form. It is observed from the figure that compound **8d** binds from a region close to the C chain region of dimeric PLpro, while compounds **8b, 8c, 8f**, **8g, 8h** and **8k** bind more closely to the A chain region of PLpro. It is noteworthy that the binding orientations of these three compounds are almost identical. The binding orientation of compound 8d is in the same direction as these three compounds, but in opposite directions due to its binding to the A chain region, as expected. In a brief, it can be said that the binding orientations of the curcumin derivatives on the PLpro monomer chain are very similar. On the other hand, examining the binding orientations of the

Table 5
Interacting residues of PLpro with compounds 8d, 8f, 8g, 8h, Remdesivir and VIR250 and the molecular interaction types.

Compounds	Binding Affinity	Hydrogen Bond	Electrostatic	Hydrophobic	Halogen	Unfavourable
8b		1 A:Gly163^{CaHB} 1 A:Asp164^{CaHB} 1 A:Pro248^{CaHB}	1 A:Asp164^{PiA}	1 A:Tyr264^{PT} 1 C:Tyr207^{PT} 1 C:Leu185^{A} 1 C:Leu199^{A} 1 A:Pro248^{PA} 1 A:Tyr264^{PA} 1 C:Tyr207^{PA}		
8c		1 A:Asp164^{CaHB}	1 A:Asp164^{PiA}	1 A:Tyr264^{PT} 1 C:Tyr207^{PT} 1 C:Leu185^{A} 1 C:Leu199^{A} 1 A:Pro248^{PA} 1 A:Tyr264^{PA} 1 C:Tyr207^{PA}		
8d	-9.5	1 C:Glu167^{CaHB} 1 C:Pro248^{CaHB} 1 C:Thr301^{CoHB} 1 A:Met208^{PdHB}	1 C:Glu161^{PiA} 1 C:Asp164^{PiA}	1 C:Tyr264^{PT} 1 A:Tyr207^{PT} 1 C:Pro248^{PA} 1 C:Tyr264^{PA}	1 A:Met206	
8f	-9.5	1 A:Pro248^{CaHB}	1 A:Glu161^{PiA} 1 A:Asp164^{PiA}	1 A:Tyr264^{PT} 1 C:Leu185^{A} 1 C:Leu199^{A} 1 A:Pro248^{PA} 1 A:Tyr264^{PA} 1 C:Tyr207^{PA}		
8g	-9.6	1 A:Pro248^{CaHB}	1 A:Glu161^{PiA} 1 A:Asp164^{PiA}	1 A:Tyr264^{PT} 1 C:Tyr207^{PT} 1 C:Leu185^{A} 1 C:Leu199^{A} 1 A:Pro248^{PA} 1 A:Tyr264^{PA} 1 C:Tyr207^{PA}		
8h	-9.6	1 A:Gly163^{CaHB} 1 A:Asp164^{CaHB} 1 A:Pro248^{CaHB} 1 C:Tyr207^{CaHB}	1 A:Asp164^{PiA}	1 A:Tyr264^{PT} 1 C:Tyr207^{PT} 1 A:Pro248^{PA} 1 A:Tyr264^{PA}	1 C:Met206 1 A:Glu161	
8k		1 C:Met206^{CoHB} 1 A:Glu161^{CoHB} 1 A:Glu167^{CaHB}	1 A:Asp164^{PiA}	1 A:Tyr264^{PT} 1 A:Pro248^{PA} 1 A:Tyr264^{PA}		
Remdesivir	-8.8	1 A:Tyr268^{CoHB} 1 A:Ala246^{CoHB} 1 C:Arg166^{CoHB} 1 C:Thr301^{CoHB}	1 C:Asp164^{Att}	2 A:Tyr264^{PT} 1 C:Arg166^{A} 1 C:Met208^{A} 1 C:Pro248^{A} 1 A:Pro248^{PA} 1 C:Pro247^{PA} 2 C:Tyr264^{PA}		2 C:Arg166, 1 A:Arg166
VIR250	-7.6	2 C:Asp164^{CoHB} 1 A:Arg166^{CoHB} 4 C:Arg166^{CoHB} 1 C:Thr301^{CoHB} 1 A:Pro248^{CaHB}	2 A:Asp164^{PiA}	2 A:Pro248^{PA}		1 C:Arg166

CaHB: Carbon Hydrogen Bond, CoHB: Conventional Hydrogen Bond, PdHB: Pi-Donor Hydrogen Bond, Att: Attractive Charge, PiA: Pi-Anion, PiCa: Pi-Cation, PS: Pi-Pi Stacked, PiS: Pi-Sigma, PT: Pi-Pi T-shaped, A: Alkly, PA: Pi-Alkyl.

reference drug Remdesivir and the PLpro enzyme inhibitor VIR250, it is seen that they interact with both monomer (chain A and chain C) chains of dimeric PLpro. Thus, although the binding orientation of Remdesivir and VIR250 is similar each other, they are almost perpendicular to the binding orientation of curcumin derivatives with high affinity. In summary, when it is considered together with these observed findings regarding binding orientations and the fact that compounds **8b, 8c, 8d**, **8f**, **8g, 8h** and **8k** have higher affinity for the PLpro enzyme than Remdesivir and VIR250, the results point out that it is necessary to focus on compounds and their derivatives that will interact with a single monomer chain of PLpro to design more effective PLpro enzyme inhibitors in future studies.

3.3. MD simulations and MM-PBSA analysis

Docking simulations are performed in a vacuum environment, and the target protein structures are kept rigid while the ligands move during these kinds of simulations. However, in physiological conditions, both target proteins and ligands interact dynamically in the solution environment. Therefore, MD simulations need to be performed in environments close to physiological conditions for protein-ligand complexes obtained as a result of docking simulations. Thanks to the simulations, it is possible to investigate the effect of ligands (small molecules) on the conformation of the target structure. In addition, MM-PBSA analysis using simulation data enables it possible to evaluate binding stability, dominant interaction types in binding, and the residues that play a critical role in binding.

In this context, the dimeric PLpro enzyme, which has the highest docking affinity value trend for curcumin derivatives, was selected as the target protein structure in our MD simulations. Curcumin derivatives some of **8b, 8c**, **8d**, **8f**, **8g, 8h** and **8k**, which have the highest docking score for this enzyme, VIR250 as the enzyme inhibitor, and Remdesivir as the reference drug were selected as the ligands. MD simulations of 100 ns were performed for 9 relevant PLpro-ligand complexes. In addition, the wild-type (wt) form of the PLpro enzyme was simulated to make a comparison with the PLpro-ligand complexes.

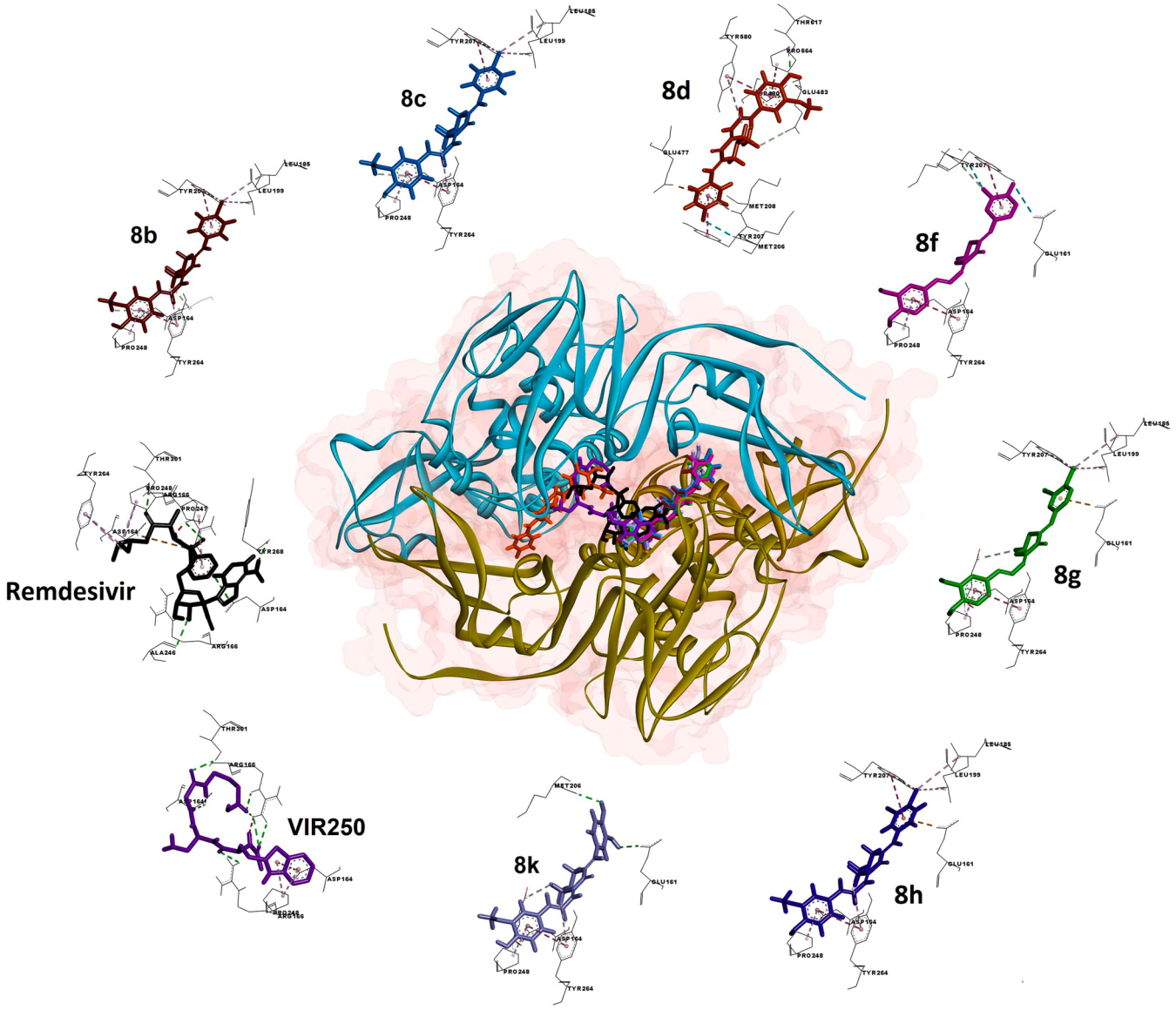

Fig. 3. 3D representations of the interactions of compounds 8b, 8c, 8d, 8 f, 8 g, 8 h, 8k, Remdesivir, and VIR250, and 3D superimposed representations of their binding sites on the dimeric PLpro target structure.

Firstly, RMSF analysis was performed with the data obtained from the MD simulation to examine the effect of ligands on the conformation of the dimeric PLpro enzyme. This analysis gives a measure of how far each residue in the PLpro enzyme moves away from its reference location, on average, over the course of the simulations. In other words, performing this analysis makes it possible to detect mobile and stable residues or residue regions in the enzyme. Accordingly, Fig. 4 shows the RMSF values per residue calculated for each monomer chain of PLpro, separately. The figure also includes the 3D structure of the dimeric and monomeric PLpro enzymes to better understand the mobile and stable regions, based on the RMSF results.

The results show that the 1–75 residue region (N-terminal) in both PLpro chains has quite high RMSF values and thus indicating that this residue region is very flexible. As can be seen from the 3D figure (residues shown in green), this residue region is located farther outside the central (core/buried) amino acid regions where monomers interact with each other, and conformation stabilizes due to these interactions. In other words, this region, which is outside the core region of the protein, has a surface area that can interact more with the solution. For this reason, it can be an expected result that this residue region will be more mobile and flexible. Upon examination of the RMSF values of other amino acids and amino acid regions, it can be assumed that the 186–196, 222–231, and 268–270 residue regions are mobile since they exceed the RMSF value of 0.2 nm for both chains of PLpro enzyme. These mobile regions are depicted in Fig. 4 in blue, red, and pink, respectively. Here, the ligand binding cavity region located between 2 monomer chains, depicted with the black circle on the 3D figure, seems to be more stable in the dimeric PLpro structure.

In addition, Fig. 5 represents the relative RMSF values calculated to examine the inhibition effect of the ligands on the conformational structure of the PLpro enzyme in more detail. For these calculations, RMSF values per residue obtained for each ligand-PLpro complex were subtracted from RMSF values per residue obtained for wt-PLpro. Accordingly, the high positive and negative values obtained in the relative RMSF chart can be considered as an indicator of deterioration or inhibition in the PLpro conformation. It is seen in the figure that the majority of relative RMSF values obtained for the entire ligand-PLpro complex are positive. Many shoulders on the figure are also seen, corresponding to regions where ligands have greater effect on PLpro conformation. Here, significant shoulder areas are circled and named in

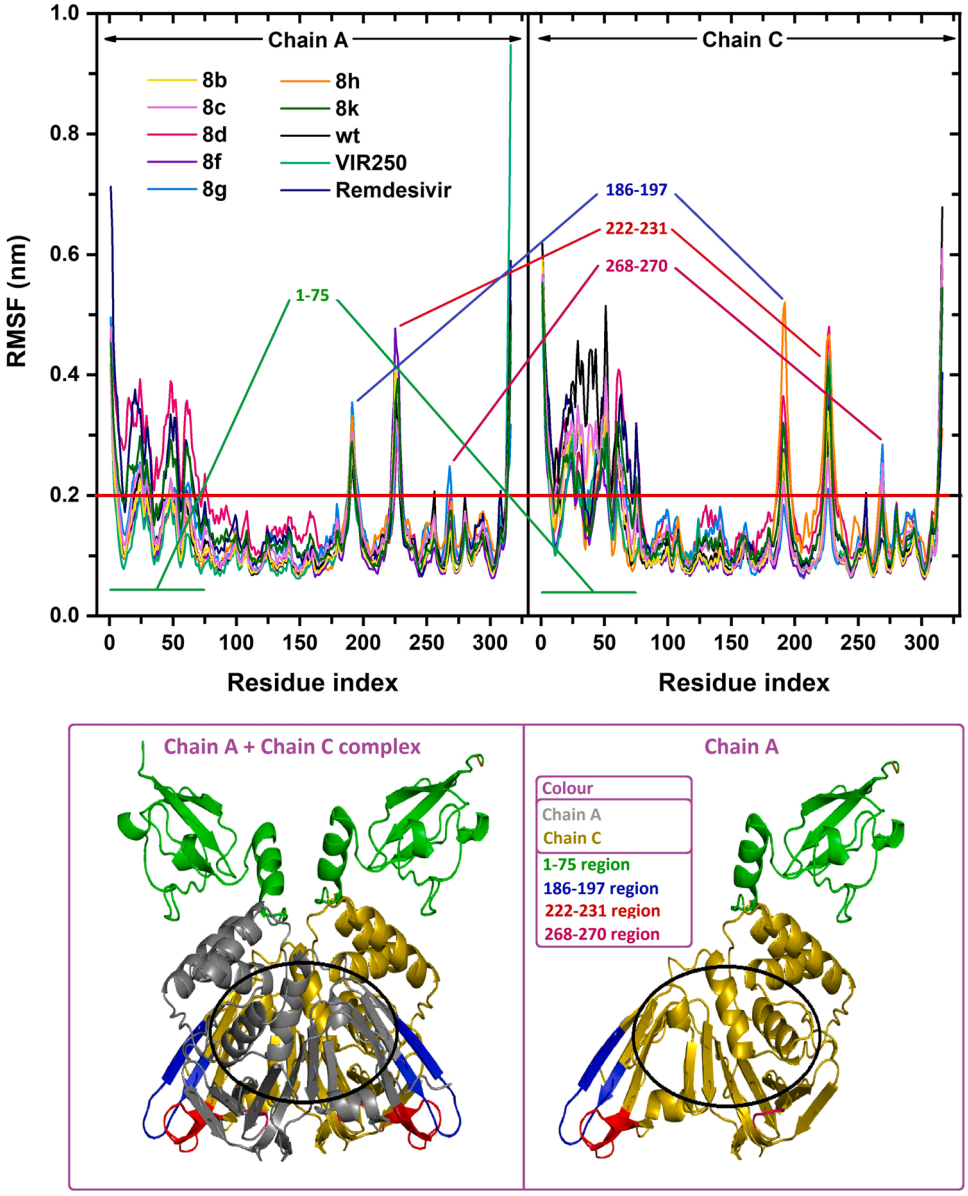

Fig. 4. The calculated RMSF values per-residue for dimeric PLpro enzymes in wt system and 8b/8c/8d/8 f/8 g/8 h/8k/Remdesivir/VIR2507-Protein complexes. 3D conformational structure of dimeric (Chain A + Chain C complex) and monomeric (only Chain A) PLpro protein. Chain A in a grey cartoon and Chain C in a yellow cartoon with some flexible residue region in different colours were represented.

the figure. All findings indicate that all ligands have a significant inhibitory effect on the conformation of the PLpro enzyme.

MM-PBSA analysis was then performed using MD simulation data to determine the dominant interaction types in dynamic binding. Table 6 shows the binding energy values calculated for each ligand-PLpro enzyme system and its components. The negative energy values in the table correspond to favorable contributions in binding energy, while the positive values correspond to unfavorable contributions. In this context, only the polar solvation energy (ΔE^{ps}) contributes negatively to ligand binding, while all other energy components contribute positively.

A comparison between the binding energy ($\Delta E^{binding}$) values in each system shows that compounds **8b**, **8c 8d**, **8f**, **8g**, **8h** and **8k** have significantly higher values than Remdesevir and VIR250.

On the other hand, the highest ΔE^{vdw} values (ΔE^{vdw} is an energy component that makes up $\Delta E^{binding}$ values) were obtained for Remdesivir, while the lowest values were obtained for VIR250. Also, a comparison among the curcumin derivatives themselves shows that their ΔE^{vdw} values increased (**8f>8g>8h** with double substituents and **8b>8c>8d** with single substituents) with increasing van der Waals diameter (Br>Cl>Fl).

The highest values for the ΔE^{elec} energy contribution were also obtained for Remdesivir, and the second largest value was obtained for VIR250. Here, **8k** is the compound with the highest electrostatic energy contribution among the curcumin derivatives. This situation can be attributed to the fact that the double hydroxy substituent of **8k** compound enhances the hydrogen bond interactions.

As is known, the sum of ΔE^{vdw} (van der Waals energy) and ΔE^{elec} (electrostatic energy) energy contributions results in molecular mechanical energy ($\Delta E^{mm} = \Delta E^{vdw} + \Delta E^{ele}$). When these terms making up the ΔE^{mm} are compared, it can be said that the van der Waals interaction energy contribution is more dominant for the systems studied. Moreover, although Remdesivir has the highest value for ΔE^{mm} energy contribution, it does not have the highest $\Delta E^{binding}$ value due to its considerably higher ΔE^{ps} negative contributions than other systems. On the other hand, it seems that the higher ΔE^{elec} value and the lower ΔE^{vdW} value of VIR250, compared to the curcumin derivatives, allow it

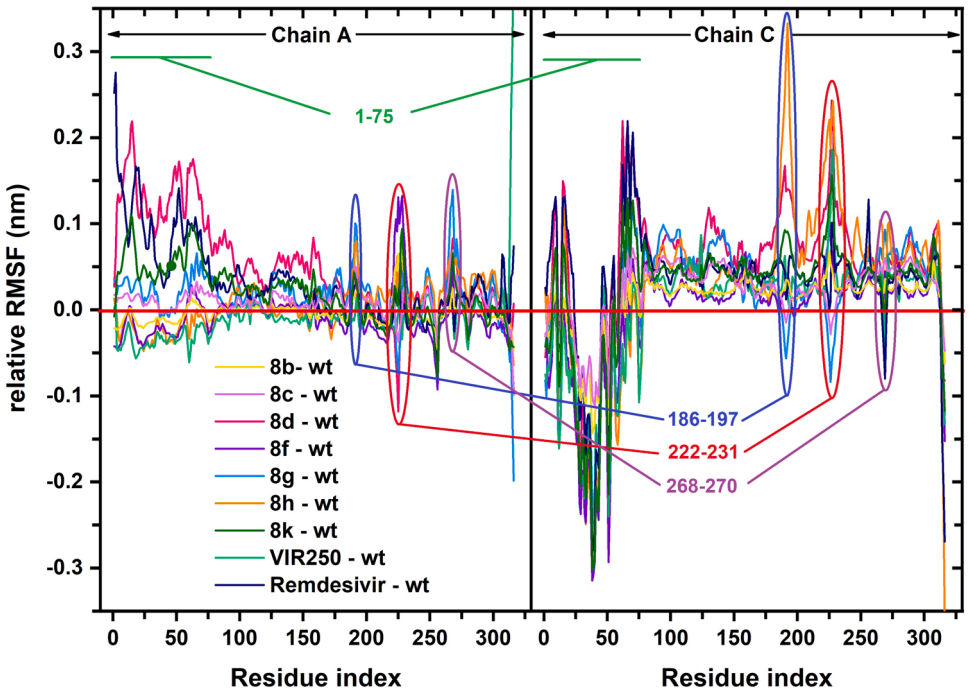

Fig. 5. The calculated relative RMSF values per-residue for dimeric PLpro enzymes in Protein and 8b/8c/8d/8 f/8 g/8 h/8k/Remdesivir/VIR2507 complexes.

Table 6
The binding free energy values and its components (kcal/mol) between ligands and dimeric PLpro complex.

	Energy (kcal/mol)					
System	ΔE^{vdW}	ΔE^{elec}	ΔE^{mm}	ΔE^{ps}	ΔE^{sasa}	$\Delta E^{binding}$
8b	-220.3	-38.9	-259.2	203.5	-18.3	-74.0
	± 13.4	± 2.9		± 13.2	± 0.9	± 4.5
8c	-211.4	-38.7	-250.1	203.4	-18.5	-65.2
	± 13.2	± 3.0		± 12.5	± 1.0	± 4.3
8d	-194.1	-29.3	-223.4	172.8	-20.1	-71.1
	± 14.3	± 4.0		± 13.5	± 1.0	± 4.4
8 f	-223.0	-39.3	-262.3	203.8	-22.2	-80.8
	± 13.7	± 2.6		± 12.9	± 0.9	± 4.6
8 g	-217.1	-38.9	-256.1	203.3	-22.6	-75.3
	± 13.1	± 2.5		± 12.3	± 0.5	± 4.5
8 h	-197.9	-30.1	-228.0	167.4	-17.2	-77.4
	± 14.7	± 3.4		± 13.3	± 1.3	± 4.7
8k	-228.5	-44.3	-272.8	233.3	-24.1	-63.6
	± 14.2	± 3.6		± 16.5	± 1.2	± 4.2
Remdesivir	-241.4	-87.9	-329.3	312.5	-28.0	-46.9
	± 13.6	± 7.4		± 23.0	± 1.2	± 4.1
VIR250	-163.6	-58.6	-222.2	205.9	-20.5	-40.2
	± 15.1	± 6.1		± 14.9	± 1.0	± 4.5

ΔE^{vdw}; van der Waals energy, ΔE^{ele}; electrostatic energy, $\Delta E^{mm} = \Delta E^{vdw} + \Delta E^{ele}$, ΔE^{ps}; polar solvation energy, ΔE^{sasa}; sasa energy, $\Delta E^{binding}$; calculated binding free energy.

to have a close ΔE^{mm} energy value to the derivatives. However, VIR250 has a lower $\Delta E^{binding}$ energy than the curcumin derivatives due to its higher negative ΔE^{ps} contribution. In summary, it can be said that the less unfavorable ΔE^{ps} energy contributions of curcumin derivatives enable them to have higher binding energies ($\Delta E^{binding}$) than Remdesivir and VIR250.

In addition, binding energy contribution values per residue were calculated, as shown in Fig. S33-41 separately, for each system in order to observe the energy contributions in ligands binding of each residue in the dimeric form of the PLpro enzyme. Here, it can be said that ligands play a key role in binding to target enzymes for residues with values of $\geq +0.5$ or ≤ -0.5 kcal/mol. This is because these relatively high positive and negative energy contributions, provided by residues in binding, can be directly associated with the conformational inhibition of the target structure. Residues with an energy contribution of $\geq +0.5$ or ≤ -0.5 kcal/mol are shown by their names on Fig. S33-41. Accordingly, residues with an energy contribution of $\geq +0.5$ kcal/mol are henceforth named hot residues and those with an energy contribution ≥ -0.5 kcal/mol are termed un-hot residues in this study. According to the Fig. S33-S41, it is observed that there are many common hot and un-hot residues that interact with the PLpro enzyme for all ligands.

In this regard, Table 7 lists the hot and un-hot residues in each monomer chain of PLpro in the systems in order to show a more detailed and convenient examination of hot and un-hot residues in the dimeric PLpro enzyme. Here, if any residue of the PLpro in a complex system is hot/un-hot, the energy contribution values of that residue in all ligand-PLpro complexes were also added to Table 6. The purpose here is to make it easier to understand common hot/un-hot PLpro residues in the complexes and to identify differences between the complex systems. In addition, the detection of common hot and un-hot residuals in the ligand-dimeric PLpro enzyme systems is of great importance for identifying key residues in ligand binding to the dimeric PLpro enzyme. In this study, we focused on the assumption that residues exceeding the threshold of $\geq +0.5$ or ≤ -0.5 kcal/mol in common in at least 5 of the 9 systems may be key residues.

Accordingly, as shown in Table 6, the residue Lys157 is an un-hot residue in binding to compounds **8b**, **8d**, **8 f**, **8 h** and **8k,** while it is a hot residue in binding to compound **8 g** and Remdesivir; hence, it can be considered as one of the residues that play a key role in ligand binding to PLpro as both a hot and an un-hot residue.

Examining the common un-hot residues, it seems that the residue Asp164 has negative energy contributions with all of 9 systems. Also, the Arg166 has un-hot negative energy contributions with 8 of 9 systems except for **8 g**. On the other hand, the Glu167 has negative energy contributions with 7 of 9 systems in all systems (except for **8 g** and Remdesivir). Furthermore, the residue Glu161 has un-hot energy contributions with 6 of 9 systems (**8b**, **8c, 8d 8 f**, **8 h**, and **8k**), similarly Asp302 is an un-hot residue with 6 of 9 systems (**8b**, **8c, 8 f**, **8 h**, Remdesivir, and VIR250). In addition, the residues Tyr273 appear to be un-hot residues with negative contributions to **8c**, **8d**, **8 f**, **8 h** and **8k**.

Examining the hot residues, which positively contribute to binding

Table 7
Hot and unhot residues in each monomer chain of PLpro in protein-ligand complexes.

	8b		8c		8d		8f		8g		8h		8k		Remdesivir		VIR250	
	A	C	A	C	A	C	A	C	A	C	A	C	A	C	A	C	A	B
Arg82	-0.09	-0.06	-0.24	-0.12	0.07	0.17	-0.25	-0.18	0.10	0.08	**-0.55**	-0.30	-0.09	0.00	-0.11	-0.06	0.07	0.07
Asp108	0.23	0.08	0.24	0.12	0.00	-0.07	0.47	0.19	-0.09	-0.02	0.50	0.27	0.24	0.06	-0.04	0.02	-0.02	-0.04
Lys157	0.65	-0.14	0.28	-0.22	0.00	3.07	0.88	-0.34	1.35	0.14	0.15	**-0.50**	0.44	1.37	**-0.58**	-0.08	0.41	0.07
Glu161	0.58	0.09	0.60	0.16	0.03	0.81	1.24	0.24	-0.23	-0.02	1.29	0.39	0.64	0.53	0.16	0.00	-0.09	-0.07
Leu162	-0.26	-0.02	**-0.70**	-0.02	0.01	-0.36	-0.37	0.01	-0.16	0.00	**-1.25**	0.00	-0.18	-0.18	-0.02	-0.12	-0.14	-0.04
Asp164	2.15	1.85	2.85	1.91	-0.08	1.16	1.00	0.41	1.09	-0.37	2.40	0.53	0.46	0.79	4.04	1.15	3.29	3.28
Arg166	1.14	2.18	1.43	1.39	1.72	0.38	-0.40	1.43	1.28	1.70	0.18	-0.15	0.66	0.91	0.46	2.43	2.68	2.93
Glu167	0.54	0.00	0.68	0.13	-0.15	0.88	0.58	0.27	-0.26	-0.47	0.85	0.52	0.22	0.58	-0.09	-0.06	0.50	-0.27
Arg183	-0.12	0.26	-0.19	-0.26	0.77	-0.02	-0.26	0.36	0.03	0.25	-0.40	**-0.67**	0.26	0.17	0.05	-0.19	0.03	0.15
Glu203	0.09	0.12	0.18	0.44	-0.28	0.00	0.23	0.29	-0.05	-0.28	0.41	0.94	-0.03	0.15	0.06	0.34	-0.05	-0.06
Tyr207	-0.01	-0.37	0.00	-0.32	-0.42	-0.01	-0.01	**-0.72**	-0.01	-0.24	0.01	**-0.61**	-0.22	-0.37	-0.06	-0.02	-0.01	-0.02
Met208	-0.25	**-0.66**	-0.29	**-0.73**	**-1.16**	-0.06	-0.12	-0.42	-0.13	**-0.91**	-0.20	**-0.57**	**-0.64**	-0.24	**-1.49**	**-1.18**	-0.37	**-0.89**
Lys232	-0.13	0.12	-0.18	1.13	1.06	-0.05	-0.30	0.15	0.00	0.29	-0.39	2.17	0.38	0.05	0.04	-0.17	0.04	0.09
Ser245	-0.12	-0.20	-0.20	-0.15	-0.14	-0.03	-0.15	-0.12	-0.05	0.09	-0.32	-0.01	-0.15	-0.08	**-1.03**	-0.27	-0.08	-0.28
Pro247	**-0.50**	-0.43	**-0.61**	-0.49	-0.12	-0.23	-0.33	-0.10	-0.39	-0.05	**-0.59**	-0.22	-0.23	-0.17	**-1.89**	**-1.31**	**-0.63**	**-0.76**
Pro248	**-0.66**	-0.21	**-0.76**	-0.23	-0.02	**-0.54**	**-0.64**	-0.01	**-0.56**	-0.01	**-0.84**	-0.04	**-0.53**	-0.28	**-1.04**	**-1.20**	**-0.67**	-0.41
Glu263	0.07	0.10	0.25	0.15	-0.04	-0.04	0.16	0.25	-0.07	-0.07	**0.53**	0.34	0.06	0.11	-0.20	-0.06	-0.03	-0.05
Tyr264	**-0.79**	-0.17	**-0.87**	-0.18	-0.01	**-1.22**	**-0.75**	0.00	**-0.77**	-0.01	**-0.92**	-0.02	-0.38	**-0.61**	**-1.39**	**-0.76**	**-0.82**	-0.33
Tyr268	**-0.77**	-0.42	**-0.50**	-0.41	-0.02	-0.19	-0.45	-0.04	**-0.86**	-0.03	0.10	-0.02	-0.24	-0.12	-0.16	-0.44	**-1.09**	**-0.80**
Cys270	-0.09	-0.01	-0.35	-0.01	-0.01	-0.25	-0.09	-0.01	-0.07	0.00	**-0.62**	-0.01	-0.05	-0.13	-0.05	-0.04	-0.08	-0.01
Tyr273	0.38	0.09	0.55	0.09	0.00	0.56	0.59	-0.01	0.42	0.00	0.92	-0.01	0.50	0.28	-0.13	0.41	0.17	0.19
Thr301	0.42	-0.12	-0.03	-0.11	-0.06	0.30	0.52	-0.03	0.29	-0.04	-0.36	0.00	0.23	0.14	**-0.93**	0.53	0.31	-0.21
Asp302	0.69	0.65	1.53	0.85	-0.49	0.39	1.00	0.07	0.29	-0.37	2.68	0.47	0.26	0.23	4.97	1.02	0.38	1.22

Hot residues ($\geq +0.5$ kcal/mol) are in bold text while un-hot residues (≤ -0.5 kcal/mol) are in italic and underlined text.

energy, the most remarkable residues are Pro248 and Tyr264, which contribute $\geq +0.5$ kcal/mol energy in all of 9 systems. In addition, another hot residue with a key role is Met208, which exceeds the threshold value in 8 of 9 systems except for **8 f**. Also, Pro247 is an un-hot residue for **8b**, **8c**, **8 g**, Remdesivir, and VIR250.

Moreover, previous docking results showed that Glu161, Asp164, Arg166, Pro248, and Tyr264 had important and common roles in many interactions. The determination of these residues as hot/un-hot residues as a result of MM-PBSA analysis shows the reliability and dynamic bonding stability of the binding poses obtained as a result of our docking experiments.

In summary, the un-hot residues Glu161, Asp164, Arg166, Glu167, Tyr273, Asp302, the hot residues Met208, Pro247, Pro248, Tyr264 and both hot and un-hot residue Lys157 can be considered to have key roles in inhibiting the dimeric PLpro enzyme since they exceed the specified energy contribution thresholds of $\geq +0.5$ or ≤ -0.5 kcal/mol in at least 3 systems. Fig. 6 shows the locations of these residues on the dimeric PLpro enzyme conformation.

4. Conclusion

Ethnopharmacological uses of various herbs and medicinal plants are necessary for human life and health due to their extensive biological activity against diseases. Phytochemicals found in these herbs and plants are generally non-toxic and have the potential to prevent chronic ailments. It has also been extensively reported in the literature that curcumin, natural phytochemicals found in Curcuma longa, can also act as antiviral compounds that inhibit virus replication for a wide range of viruses.

In light of this information, this study focused on various curcumin derivatives that are easily synthesized and have high pharmacological properties and this regard, it was also investigated the potential of various 2 H-pyran-4(3 H)-one and 1-methylpiperidine-4-one curcumin derivatives as effective antiviral agents to inhibit COVID-19 main enzymes. In this context, 22 curcumin derivatives with good and reliable ADME profiles were identified, and then for these derivatives, molecular docking studies were performed against 3CLPro, PLpro, NSP7/8/12, NSP7/8/12 +RNA, NSP15, NSP16, Spike, Spike+ACE enzymes, which are important receptors of SARS-CoV-2. In addition, the docking binding scores obtained were compared with natural curcuminoids, various receptor inhibitors, and various drug molecules (warfarin, favipiravir, remdesivir, and hydroxychloroquine) in order to evaluate the potential of the proposed curcumin derivatives as antiviral drugs. According to the docking studies, all proposed curcumin derivatives had higher binding affinity value trend for all SARS-CoV-2 receptor targets compared to natural curcuminoids, reference enzyme inhibitors, and drug molecules. In addition, among all of the receptors studied, the highest docking scores for the proposed curcumin derivatives were obtained for the PLpro protein enzyme. The docking simulations on the PLpro target showed that the docking scores obtained for all curcumin derivatives were higher than natural curcuminoids, all reference drug molecules (warfarin (−8.0 kcal/mol), favipiravir (−5.7 kcal/mol), hydroxychloroquine (−6.7 kcal/mol), remdesivir (−8.8 kcal/mol)), and PLpro enzyme inhibitor VIR250 (−7.6 kcal/mol). Although it was observed that the binding affinity values obtained for the 22 proposed curcumin derivatives were also quite similar to each other, the highest docking score was obtained for compounds **8 g** and **8 h** with − 9.6 kcal/mol, followed by compounds **8 f** and **8d** with − 9.5 kcal/mol.

Finally, MD simulations of 100 ns were performed between PLpro complexes and compounds **8d**, **8 f**, **8 g**, **8 h**, VIR250 and Remdesivir. The effects of these ligands on the conformation of PLpro were initially observed using RMSF analysis. Later, an MM-PBSA analysis was performed using the data from the MD simulation and it was found that van der Waals interactions were the dominant type of interaction in ligand binding to PLpro. Moreover, MM-PBSA analysis showed that the residues Lys157, Glu161, Asp164, Arg166, Glu167, Met208, Pro247,

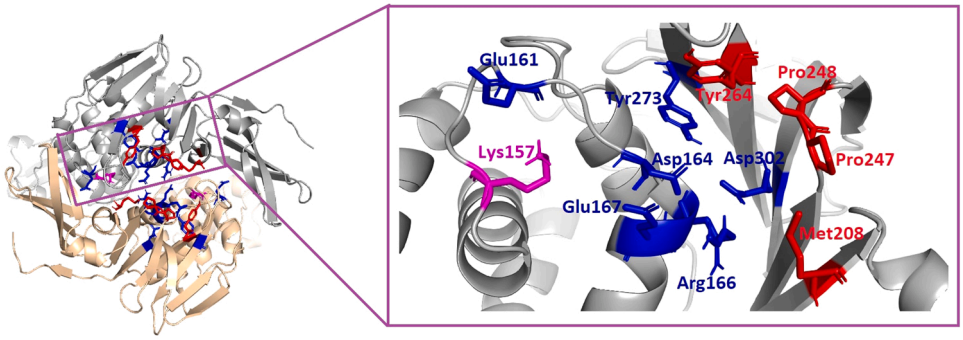

Fig. 6. Hot, un-hot residues on dimeric PLpro. Chain A in a grey cartoon and Chain C in a yellow cartoon with hot residues in red, un-hot residues in blue, and both hot and unhot residue in pink were represented.

Pro248, Tyr264, Tyr273, and Asp302 of PLpro played a key role in ligand binding to PLpro.

To conclude, the findings in the present computational study can be adapted and/or guide experimental research for the development of antiviral drugs with more potential for various enzyme receptors of SARS-CoV-2, primarily PLpro.

CRediT authorship contribution statement

Hakan Alıcı: Conceptualization, Methodology, Software, Investigation, Formal analysis, Visualization, Supervision **Kadir Demir**: Writing – review & editing **Hakan Tahtacı**: Conceptualization, Writing – review & editing.

Declaration of Competing Interest

The authors declare that they have no known competing financial interests or personal relationships that could have appeared to influence the work reported in this paper.

Data Availability

Data will be stored in our computer lab for 2 years and will be provided if anyone in need.

Acknowledgments

This work was supported by the Scientific Research Fund of Zonguldak Bülent Ecevit University with project number 2015-22794455-03, and the numerical calculations reported in this paper were performed at TUBITAK ULAKBIM, High Performance and Grid Computing Center (TRUBA resources).

Docking data

ACD/ChemSketch was utilized for the 2D chemical drawing and editing in the SDF format for all compounds. Then, using these 2D structures, various in silico absorption, distribution, metabolism, excretion (ADME) and drug-likenesses properties of the compounds were investigated using the SwissADME webserver and TCMSP webserver.

Molecular simulation (MD) data

MD simulations were performed by GROMACS program version 2020.1. In the MD simulations, CHARMM36 force field and TIP3P(Jorgensen et al., 1983) water model were used for the protein and the explicit solvent, respectively. The CHARMM36 force field parameters for ligand were derived from CHARMM General Force Field (CGenFF) web server.

Appendix A. Supporting information

Supplementary data associated with this article can be found in the online version at doi:10.1016/j.compbiolchem.2022.107657.

References

Abdusalam, A.A.A., Murugaiyah, V., 2020. Identification of potential inhibitors of 3CL protease of SARS-CoV-2 from ZINC database by molecular docking-based virtual screening. Front. Mol. Biosci. 7, 603037.

Abraham, M.J., Murtola, T., Schulz, R., Páll, S., Smith, J.C., Hess, B., Lindahl, E., 2015. GROMACS: high performance molecular simulations through multi-level parallelism from laptops to supercomputers. SoftwareX 1–2, 19–25.

Adams, B.K., Ferstl, E.M., Davis, M.C., Herold, M., Kurtkaya, S., Camalier, R.F., Hollingshead, M.G., Kaur, G., Sausville, E.A., Rickles, F.R., Snyder, J.P., Liotta, D.C., Shoji, M., 2004. Synthesis and biological evaluation of novel curcumin analogs as anti-cancer and anti-angiogenesis agents. Bioorg. Med. Chem. 12, 3871–3883.

Adelusi, T.I., Oyedele, A.-Q.K., Monday, O.E., Boyenle, I.D., Idris, M.O., Ogunlana, A.T., Ayoola, A.M., Fatoki, J.O., Kolawole, O.E., David, K.B., Olayemi, A.A., 2022. Dietary polyphenols mitigate SARS-CoV-2 main protease (Mpro)–Molecular dynamics, molecular mechanics, and density functional theory investigations. J. Mol. Struct. 1250, 131879.

Aggarwal, B.B., Shishodia, S., Takada, Y., Banerjee, S., Newman, R.A., Bueso-Ramos, C. E., Price, J.E., 2005. Curcumin suppresses the paclitaxel-induced nuclear factor-κB pathway in breast cancer cells and inhibits lung metastasis of human breast cancer in nude mice. Clin. Cancer Res. 11, 7490–7498.

Ak, T., Gülçin, İ., 2008. Antioxidant and radical scavenging properties of curcumin. Chem. Biol. Interact. 174, 27–37.

Ali, A., Banerjea, A.C., 2016. Curcumin inhibits HIV-1 by promoting Tat protein degradation. Sci. Rep. 6, 27539.

Anand, P., Kunnumakkara, A.B., Newman, R.A., Aggarwal, B.B., 2007. Bioavailability of curcumin: problems and promises. Mol. Pharm. 4, 807–818.

Astinfeshan, M., Rasmi, Y., Kheradmand, F., Karimipour, M., Rahbarghazi, R., Aramwit, P., Nasirzadeh, M., Daeihassani, B., Shirpoor, A., Gholinejad, Z., Saboory, E., 2019. Curcumin inhibits angiogenesis in endothelial cells using downregulation of the PI3K/Akt signaling pathway. Food Biosci. 29, 86–93.

Azam, F., 2021. Elucidation of teicoplanin interactions with drug targets related to COVID-19. Antibiotics 10, 10.

Badavath, V.N., Baysal, İ., Ucar, G., Sinha, B.N., Jayaprakash, V., 2016a. Monoamine oxidase inhibitory activity of novel pyrazoline analogues: curcumin based design and synthesis. ACS Med. Chem. Lett. 7, 56–61.

Badavath, V.N., Baysal, İ., Uçar, G., Mondal, S.K., Sinha, B.N., Jayaprakash, V., 2016b. Monoamine oxidase inhibitory activity of ferulic acid amides: curcumin-based design and synthesis. Arch. Pharm. 349, 9–19.

Badavath, V.N., Ucar, G., Sinha, B.N., Mondal, S.K., Jayaprakash, V., 2016c. Monoamine oxidase inhibitory activity of novel pyrazoline analogues: curcumin based design and synthesis-II. ChemistrySelect 1, 5879–5884.

Badavath, V.N., Kumar, A., Samanta, P.K., Maji, S., Das, A., Blum, G., Jha, A., Sen, A., 2020. Determination of potential inhibitors based on isatin derivatives against SARS-CoV-2 main protease (mpro): a molecular docking, molecular dynamics and structure-activity relationship studies. J. Biomol. Struct. Dyn. 1–19. https://doi.org/10.1080/07391102.2020.1845800.

Balasubramanian, A., Pilankatta, R., Teramoto, T., Sajith, A.M., Nwulia, E., Kulkarni, A., Padmanabhan, R., 2019. Inhibition of dengue virus by curcuminoids. Antivir. Res. 162, 71–78.

Benet, L.Z., Hosey, C.M., Ursu, O., Oprea, T.I., 2016. BDDCS, the rule of 5 and drugability. Adv. Drug Deliv. Rev. 101, 89–98.

Berman, H.M., Westbrook, J., Feng, Z., Gilliland, G., Bhat, T.N., Weissig, H., Shindyalov, I.N., Bourne, P.E., 2000. The protein data bank. Nucleic Acids Res. 28, 235–242.

Bickerton, G.R., Paolini, G.V., Besnard, J., Muresan, S., Hopkins, A.L., 2012. Quantifying the chemical beauty of drugs. Nat. Chem. 4, 90–98.

Bussi, G., Donadio, D., Parrinello, M., 2007. Canonical sampling through velocity rescaling. J. Chem. Phys. 126, 014101.

Bykhovskaya, O.V., Aladzheva, I.M., Makarov, M.V., Rybalkina, E.Y., Klemenkova, Z.S., Brel, V.K., 2017. Synthesis and study of antitumor activity of 4H-pyrano[3,2-c]pyridines based on N-(2-azidoethyl)- and N-propargyl-3,5-bis(arylidene)piperidin-4-ones. Russ. Chem. Bull. 66, 104–110.

C, S., S, D.K., Ragunathan, V., Tiwari, P., A, S., P, B.D., 2022. Molecular docking, validation, dynamics simulations, and pharmacokinetic prediction of natural compounds against the SARS-CoV-2 main-protease. J. Biomol. Struct. Dyn. 40, 585–611.

Cao, Y., Li, L., Feng, Z., Wan, S., Huang, P., Sun, X., Wen, F., Huang, X., Ning, G., Wang, W., 2020. Comparative genetic analysis of the novel coronavirus (2019-nCoV/SARS-CoV-2) receptor ACE2 in different populations. Cell Discov. 6, 11.

Choudhary, N., Singh, V., 2022. Multi-scale mechanism of antiviral drug-alike phytoligands from Ayurveda in managing COVID-19 and associated metabolic comorbidities: insights from network pharmacology. Mol. Divers. 7, 1–20.

Cianciulli, A., Calvello, R., Porro, C., Trotta, T., Salvatore, R., Panaro, M.A., 2016. PI3k/Akt signalling pathway plays a crucial role in the anti-inflammatory effects of curcumin in LPS-activated microglia. Int. Immunopharmacol. 36, 282–290.

Dai, J., Gu, L., Su, Y., Wang, Q., Zhao, Y., Chen, X., Deng, H., Li, W., Wang, G., Li, K., 2018a. Inhibition of curcumin on influenza A virus infection and influenzal pneumonia via oxidative stress, TLR2/4, p38/JNK MAPK and NF-κB pathways. Int. Immunopharmacol. 54, 177–187.

Dai, W., Wang, H., Fang, J., Zhu, Y., Zhou, J., Wang, X., Zhou, Y., Zhou, M., 2018b. Curcumin provides neuroprotection in model of traumatic brain injury via the Nrf2-ARE signaling pathway. Brain Res. Bull. 140, 65–71.

Daina, A., Michielin, O., Zoete, V., 2014. iLOGP: a simple, robust, and efficient description of n-octanol/water partition coefficient for drug design using the GB/SA approach. J. Chem. Inf. Model. 54, 3284–3301.

Daina, A., Michielin, O., Zoete, V., 2017. SwissADME: a free web tool to evaluate pharmacokinetics, drug-likeness and medicinal chemistry friendliness of small molecules. Sci. Rep. 7, 42717.

Dallakyan, S., Olson, A.J., 2015. Small-molecule library screening by docking with PyRx. In: Hempel, J.E., Williams, C.H., Hong, C.C. (Eds.), Chemical Biology: Methods and Protocols. Springer, New York, New York, NY, pp. 243–250.

Donoghue, M., Hsieh, F., Baronas, E., Godbout, K., Gosselin, M., Stagliano, N., Donovan, M., Woolf, B., Robison, K., Jeyaseelan, R., Breitbart Roger, E., Acton, S., 2000. A novel angiotensin-converting enzyme–related carboxypeptidase (ACE2) converts angiotensin I to angiotensin 1-9. Circ. Res. 87, e1–e9.

Du, T., Shi, Y., Xiao, S., Li, N., Zhao, Q., Zhang, A., Nan, Y., Mu, Y., Sun, Y., Wu, C., Zhang, H., Zhou, E.-M., 2017. Curcumin is a promising inhibitor of genotype 2 porcine reproductive and respiratory syndrome virus infection. BMC Vet. Res. 13, 298.

Egan, W.J., Merz, K.M., Baldwin, J.J., 2000. Prediction of drug absorption using multivariate statistics. J. Med. Chem. 43, 3867–3877.

Elhady, S.S., Abdelhameed, R.F.A., Malatani, R.T., Alahdal, A.M., Bogari, H.A., Almalki, A.J., Mohammad, K.A., Ahmed, S.A., Khedr, A.I.M., Darwish, K.M., 2021. Molecular docking and dynamics simulation study of Hyrtios erectus isolated scalarane sesterterpenes as potential SARS-CoV-2 dual target Inhibitors. Biology 10, 389.

Fawzy, I.M., Youssef, K.M., Ismail, N.S.M., Gullbo, J., Abouzid, K.A.M., 2015. Design, synthesis and biological evaluation of novel curcumin analogs with anticipated anticancer activity. Future. J. Pharm. Sci. 1, 22–31.

Ferreira, V.H., Nazli, A., Dizzell, S.E., Mueller, K., Kaushic, C., 2015. The anti-inflammatory activity of curcumin protects the genital mucosal epithelial barrier from disruption and blocks replication of HIV-1 and HSV-2. Plos One 10, e0124903.

Ganesh, P., Karthikeyan, R., Muthukumaraswamy, A., Anand, J., 2017. A potential role of periodontal inflammation in Alzheimer's disease: a review. Oral. Health Prev. Dent. 15, 7–12.

Gangadevi, S., Badavath, V.N., Thakur, A., Yin, N., De Jonghe, S., Acevedo, O., Jochmans, D., Leyssen, P., Wang, K., Neyts, J., Yujie, T., Blum, G., 2021. Kobophenol A inhibits binding of host ACE2 receptor with spike RBD domain of SARS-CoV-2, a lead compound for blocking COVID-19. J. Phys. Chem. Lett. 12, 1793–1802.

Gao, Y., Tai, W., Wang, N., Li, X., Jiang, S., Debnath, A.K., Du, L., Chen, S., 2019. Identification of novel natural products as effective and broad-spectrum anti-zika virus inhibitors. Viruses 11, 1019.

Ghose, A.K., Viswanadhan, V.N., Wendoloski, J.J., 1999. A knowledge-based approach in designing combinatorial or medicinal chemistry libraries for drug discovery. 1. A qualitative and quantitative characterization of known drug databases. J. Comb. Chem. 1, 55–68.

Goozee, K.G., Shah, T.M., Sohrabi, H.R., Rainey-Smith, S.R., Brown, B., Verdile, G., Martins, R.N., 2016. Examining the potential clinical value of curcumin in the prevention and diagnosis of Alzheimer's disease. Br. J. Nutr. 115, 449–465.

Gupta, S., Ravishankar, S., 2005. A comparison of the antimicrobial activity of garlic, ginger, carrot, and turmeric pastes against Escherichia coli O157:H7 in laboratory buffer and ground beef. Foodborne Pathog. Dis. 2, 330–340.

Hamming, I., Timens, W., Bulthuis, M.L.C., Lely, A.T., Navis, G.J., van Goor, H., 2004. Tissue distribution of ACE2 protein, the functional receptor for SARS coronavirus. A first step in understanding SARS pathogenesis. J. Pathog. 203, 631–637.

Hanwell, M.D., Curtis, D.E., Lonie, D.C., Vandermeersch, T., Zurek, E., Hutchison, G.R., 2012. Avogadro: an advanced semantic chemical editor, visualization, and analysis platform. J. Chemin.-. 4, 17.

Harcourt, B.H., Jukneliene, D., Kanjanahaluethai, A., Bechill, J., Severson, K.M., Smith, C.M., Rota, P.A., Baker, S.C., 2004. Identification of severe acute respiratory syndrome coronavirus replicase products and characterization of papain-like protease activity. J. Virol. 78, 13600–13612.

Hasan, A., Biswas, P., Bondhon, T.A., Jannat, K., Paul, T.K., Paul, A.K., Jahan, R., Nissapatorn, V., Mahboob, T., Wilairatana, P., Hasan, M.N., de Lourdes Pereira, M., Wiart, C., Rahmatullah, M., 2022. Can Artemisia herba-alba Be Useful for Managing COVID-19 and Comorbidities? Molecules 27, 492.

Hess, B., 2008. P-LINCS: a parallel linear constraint solver for molecular simulation. J. Chem. Theory Comput. 4, 116–122.

Hoffmann, M., Kleine-Weber, H., Schroeder, S., Krüger, N., Herrler, T., Erichsen, S., Schiergens, T.S., Herrler, G., Wu, N.-H., Nitsche, A., Müller, M.A., Drosten, C., Pöhlmann, S., 2020. SARS-CoV-2 cell entry depends on ACE2 and TMPRSS2 and is blocked by a clinically proven protease inhibitor. Cell 181, 271–280 e278.

Huang, C., Wang, Y., Li, X., Ren, L., Zhao, J., Hu, Y., Zhang, L., Fan, G., Xu, J., Gu, X., Cheng, Z., Yu, T., Xia, J., Wei, Y., Wu, W., Xie, X., Yin, W., Li, H., Liu, M., Xiao, Y., Gao, H., Guo, L., Xie, J., Wang, G., Jiang, R., Gao, Z., Jin, Q., Wang, J., Cao, B., 2020. Clinical features of patients infected with 2019 novel coronavirus in Wuhan, China. Lancet 395, 497–506.

Huang, H.-I., Chio, C.-C., Lin, J.-Y., 2018. Inhibition of EV71 by curcumin in intestinal epithelial cells. PLos One 13, e0191617.

Huang, J., MacKerell Jr, A.D., 2013. CHARMM36 all-atom additive protein force field: Validation based on comparison to NMR data. J. Comput. Chem. 34, 2135–2145.

Huey, R., Morris, G.M., Olson, A.J., Goodsell, D.S., 2007. A semiempirical free energy force field with charge-based desolvation. J. Comput. Chem. 28, 1145–1152.

Jennings, M.R., Parks, R.J., 2020. Curcumin as an antiviral agent. Viruses 12, 1242.

Jeong, E.-H., Vaidya, B., Cho, S.-Y., Park, M.-A., Kaewintajuk, K., Kim, S.R., Oh, M.-J., Choi, J.-S., Kwon, J., Kim, D., 2015. Identification of regulators of the early stage of viral hemorrhagic septicemia virus infection during curcumin treatment. Fish Shellfish Immunol. 45, 184–193.

Jha, A., Zhao, J., Stanley Cameron, T., De Clercq, E., Balzarini, J., Manavathu, E.K., Stables, J.P., 2006. Design, synthesis and biological evaluation of novel curcumin analogues as anti-neoplastic agents. Lett. Drug Des. Discov. 3, 304–310.

Jiang, S., Han, J., Li, T., Xin, Z., Ma, Z., Di, W., Hu, W., Gong, B., Di, S., Wang, D., Yang, Y., 2017. Curcumin as a potential protective compound against cardiac diseases. Pharmacol. Res. 119, 373–383.

Jin, Z., Du, X., Xu, Y., Deng, Y., Liu, M., Zhao, Y., Zhang, B., Li, X., Zhang, L., Peng, C., Duan, Y., Yu, J., Wang, L., Yang, K., Liu, F., Jiang, R., Yang, X., You, T., Liu, X., Yang, X., Bai, F., Liu, H., Liu, X., Guddat, L.W., Xu, W., Xiao, G., Qin, C., Shi, Z., Jiang, H., Rao, Z., Yang, H., 2020. Structure of Mpro from SARS-CoV-2 and discovery of its inhibitors. Nature 582, 289–293.

Jorgensen, W.L., Chandrasekhar, J., Madura, J.D., Impey, R.W., Klein, M.L., 1983. Comparison of simple potential functions for simulating liquid water. J. Chem. Phys. 79, 926–935.

Jovanovic, S.V., Steenken, S., Boone, C.W., Simic, M.G., 1999. H-atom transfer is a preferred antioxidant mechanism of curcumin. J. Am. Chem. Soc. 121, 9677–9681.

Kim, D., Lee, J.-Y., Yang, J.-S., Kim, J.W., Kim, V.N., Chang, H., 2020. The architecture of SARS-CoV-2 transcriptome. Cell 181, 914–921 e910.

Kim, Y., Wower, J., Maltseva, N., Chang, C., Jedrzejczak, R., Wilamowski, M., Kang, S., Nicolaescu, V., Randall, G., Michalska, K., Joachimiak, A., 2021. Tipiracil binds to uridine site and inhibits Nsp15 endoribonuclease NendoU from SARS-CoV-2. Commun. Biol. 4, 193.

Kocaadam, B., Şanlier, N., 2017. Curcumin, an active component of turmeric (Curcuma longa), and its effects on health. Crit. Rev. Food Sci. Nutr. 57, 2889–2895.

Kong, R., Yang, G., Xue, R., Liu, M., Wang, F., Hu, J., Guo, X., Chang, S., 2020. COVID-19 docking server: a meta server for docking small molecules, peptides and antibodies against potential targets of COVID-19. Bioinformatics 36, 5109–5111.

Koroth, J., Nirgude, S., Tiwari, S., Gopalakrishnan, V., Mahadeva, R., Kumar, S., Karki, S. S., Choudhary, B., 2019. Investigation of anti-cancer and migrastatic properties of novel curcumin derivatives on breast and ovarian cancer cell lines. BMC Complement Altern. Med. 19, 273.

Kumar, S., Kashyap, P., Chowdhury, S., Kumar, S., Panwar, A., Kumar, A., 2020. Identification of phytochemicals as potential therapeutic agents that binds to Nsp15 protein target of coronavirus (SARS-CoV-2) that are capable of inhibiting virus replication. Phytomedicine 85, 153317.

Kumari, R., Kumar, R., Lynn, A., 2014. g_mmpbsa—A GROMACS tool for high-throughput MM-PBSA calculations. J. Chem. Inf. Model. 54, 1951–1962.

Kunnumakkara, A.B., Bordoloi, D., Padmavathi, G., Monisha, J., Roy, N.K., Prasad, S., Aggarwal, B.B., 2017. Curcumin, the golden nutraceutical: multitargeting for multiple chronic diseases. Br. J. Pharmacol. 174, 1325–1348.

Lan, J., Ge, J., Yu, J., Shan, S., Zhou, H., Fan, S., Zhang, Q., Shi, X., Wang, Q., Zhang, L., Wang, X., 2020. Structure of the SARS-CoV-2 spike receptor-binding domain bound to the ACE2 receptor. Nature 581, 215–220.

Li, H., Zhong, C., Wang, Q., Chen, W., Yuan, Y., 2019. Curcumin is an APE1 redox inhibitor and exhibits an antiviral activity against KSHV replication and pathogenesis. Antivir. Res. 167, 98–103.

Lim, K.P., Ng, L.F., Liu, D.X., 2000. Identification of a novel cleavage activity of the first papain-like proteinase domain encoded by open reading frame 1a of the coronavirus Avian infectious bronchitis virus and characterization of the cleavage products. J. Virol. 74, 1674–1685.

Lin, C.-J., Chang, L., Chu, H.-W., Lin, H.-J., Chang, P.-C., Wang, R.Y.L., Unnikrishnan, B., Mao, J.-Y., Chen, S.-Y., Huang, C.-C., 2019. High amplification of the antiviral activity of curcumin through transformation into carbon quantum dots. Small 15, 1902641.

Lipinski, C.A., Lombardo, F., Dominy, B.W., Feeney, P.J., 1997. Experimental and computational approaches to estimate solubility and permeability in drug discovery and development settings. Adv. Drug Deliv. Rev. 23, 3–25.

Lipinski, C.A., Lombardo, F., Dominy, B.W., Feeney, P.J., 2001. Experimental and computational approaches to estimate solubility and permeability in drug discovery and development settings1PII of original article: S0169–409X(96)00423–1. The article was originally published in Adv. Drug Deliv. Rev. 23 (1997) 3–25.1. Adv. Drug Deliv. Rev. 46, 3–26.

Lu, H., Stratton, C.W., Tang, Y.-W., 2020. Outbreak of pneumonia of unknown etiology in Wuhan, China: the mystery and the miracle. J. Med. Virol. 92, 401–402.
Malone, B., Urakova, N., Snijder, E.J., Campbell, E.A., 2022. Structures and functions of coronavirus replication–transcription complexes and their relevance for SARS-CoV-2 drug design. Nat. Rev. Mol. Cell Biol. 23, 21–39.
Man, S., Zhang, L., Cui, J., Yang, L., Ma, L., Gao, W., 2018. Curcumin enhances the anti-cancer effects of Paris Saponin II in lung cancer cells. Cell Prolif. 51, e12458.
Mithilesh, S., Raghunandan, D., Suresh, P.K.,2022. In-Silico Identification of Natural Compounds from Traditional Medicine as Potential Drug Leads against SARS-CoV-2 Through Virtual Screening. Proceedings of the National Academy of Sciences, India Section B: Biological Sciences.
Mitra, D., Verma, D., Mahakur, B., Kamboj, A., Srivastava, R., Gupta, S., Pandey, A., Arora, B., Pant, K., Panneerselvam, P., Ghosh, A., Barik, D.P., Mohapatra, P.K.D., 2021. Molecular docking and simulation studies of natural compounds of Vitex negundo L. against papain-like protease (PLpro) of SARS CoV-2 (coronavirus) to conquer the pandemic situation in the world. J. Biomol. Struct. Dyn. 1–22. https://doi.org/10.1080/07391102.2021.1873185.
Miyamoto, S., Kollman, P.A., 1992. Settle: an analytical version of the SHAKE and RATTLE algorithm for rigid water models. J. Comput. Chem. 13, 952–962.
Mounce, B.C., Cesaro, T., Carrau, L., Vallet, T., Vignuzzi, M., 2017. Curcumin inhibits Zika and chikungunya virus infection by inhibiting cell binding. Antivir. Res. 142, 148–157.
Moustaqil, M., Ollivier, E., Chiu, H.-P., Van Tol, S., Rudolffi-Soto, P., Stevens, C., Bhumkar, A., Hunter, D.J.B., Freiberg, A.N., Jacques, D., Lee, B., Sierecki, E., Gambin, Y., 2021. SARS-CoV-2 proteases PLpro and 3CLpro cleave IRF3 and critical modulators of inflammatory pathways (NLRP12 and TAB1): implications for disease presentation across species. Emerg. Microb. Infect. 10, 178–195.
Muegge, I., Heald, S.L., Brittelli, D., 2001. Simple selection criteria for drug-like chemical matter. J. Med. Chem. 44, 1841–1846.
Munigunti, R., Gathiaka, S., Acevedo, O., Sahu, R., Tekwani, B., Calderón, A.I., 2014. Determination of antiplasmodial activity and binding affinity of curcumin and demethoxycurcumin towards PfTrxR. Nat. Prod. Res. 28, 359–364.
Murugesan, K., Koroth, J., Srinivasan, P.P., Singh, A., Mukundan, S., Karki, S.S., Choudhary, B., Gupta, C.M., 2019. Effects of green synthesised silver nanoparticles (ST06-AgNPs) using curcumin derivative (ST06) on human cervical cancer cells (HeLa) in vitro and EAC tumor bearing mice models. Int. J. Nanomed. 14, 5257–5270.
Murugesan, S., Kottekad, S., Crasta, I., Sreevathsan, S., Usharani, D., Perumal, M.K., Mudliar, S.N., 2021. Targeting COVID-19 (SARS-CoV-2) main protease through active phytocompounds of ayurvedic medicinal plants – Emblica officinalis (Amla), Phyllanthus niruri Linn. (Bhumi Amla) and Tinospora cordifolia (Giloy) – a molecular docking and simulation study. Comput. Biol. Med. 136, 104683.
Nath, C., Badavath, V.N., Thakur, A., Ucar, G., Acevedo, O., Mohd Siddique, M.U., Jayaprakash, V., 2018. Curcumin-based pyrazoline analogues as selective inhibitors of human monoamine oxidase A. MedChemComm 9, 1164–1171.
Oluyori, A.P., Olanipekun, B.E., Adeyemi, O.S., Egharevba, G.O., Adegboyega, A.E., Oladeji, O.S., 2022. Molecular docking, pharmacophore modelling, MD simulation and in silico ADMET study reveals bitter cola constituents as potential inhibitors of SARS-CoV-2 main protease and RNA dependent-RNA polymerase. J. Biomol. Struct. Dyn. 1–16. https://doi.org/10.1080/07391102.2021.2024883.
Özdemir, M., Köksoy, B., Ceyhan, D., Sayın, K., Erçağ, E., Bulut, M., Yalçın, B., 2020. Design and in silico study of the novel coumarin derivatives against SARS-CoV-2 main enzymes. J. Biomol. Struct. Dyn. 27, 1–16.
Parrinello, M., Rahman, A., 1981. Polymorphic transitions in single crystals: a new molecular dynamics method. J. Appl. Phys. 52, 7182–7190.
Petit, J., Meurice, N., Kaiser, C., Maggiora, G., 2012. Softening the rule of five–where to draw the line? Bioorg. Med. Chem. 20, 5343–5351.
Phong, N.V., Trang, N.M., Quyen, C.T., Anh, H.L.T., Vinh, L.B., 2022. SARS-CoV-2 main protease and papain-like protease inhibition by abietane-type diterpenes isolated from the branches of Glyptostrobus pensilis using molecular docking studies. Nat. Prod. Res. 1–8. https://doi.org/10.1080/14786419.2022.2025801.
Posthuma, C.C., Nedialkova, D.D., Zevenhoven-Dobbe, J.C., Blokhuis, J.H., Gorbalenya, A.E., Snijder, E.J., 2006. Site-directed mutagenesis of the nidovirus replicative endoribonuclease NendoU exerts pleiotropic effects on the arterivirus life cycle. J. Virol. 80, 1653–1661.
Rahmani, S., Asgary, S., Askari, G., Keshvari, M., Hatamipour, M., Feizi, A., Sahebkar, A., 2016. Treatment of non-alcoholic fatty liver disease with curcumin: a randomized placebo-controlled trial. Phytother. Res. 30, 1540–1548.
Rajagopal, K., Varakumar, P., Baliwada, A., Byran, G., 2020. Activity of phytochemical constituents of Curcuma longa (turmeric) and Andrographis paniculata against coronavirus (COVID-19): an in silico approach. Future J. Pharm. Sci. 6, 104.
Randazzo, W., Aznar, R., Sánchez, G., 2016. Curcumin-mediated photodynamic inactivation of norovirus surrogates. Food Environ. Virol. 8, 244–250.
von Rhein, C., Weidner, T., Henß, L., Martin, J., Weber, C., Sliva, K., Schnierle, B.S., 2016. Curcumin and Boswellia serrata gum resin extract inhibit chikungunya and vesicular stomatitis virus infections in vitro. Antivir. Res. 125, 51–57.
Richart, S.M., Li, Y.-L., Mizushina, Y., Chang, Y.-Y., Chung, T.-Y., Chen, G.-H., Tzen, J.T.-C., Shia, K.-S., Hsu, W.-L., 2018. Synergic effect of curcumin and its structural analogue (Monoacetylcurcumin) on anti-influenza virus infection. J. Food Drug Anal. 26, 1015–1023.
Roayapalley, P.K., Dimmock, J.R., Contreras, L., Balderrama, K.S., Aguilera, R.J., Sakagami, H., Amano, S., Sharma, R.K., Das, U., 2021. Design, synthesis and tumour-selective toxicity of novel 1-[3-{3,5-Bis(benzylidene)-4-oxo-1-piperidino}-3-oxo-propyl]-4-piperidone oximes and related quaternary ammonium salts. Molecules 26, 7132.
Rohaim, M.A., El Naggar, R.F., Clayton, E., Munir, M., 2021. Structural and functional insights into non-structural proteins of coronaviruses. Microb. Pathog. 150, 104641, 104641-104641.
Rosas-Lemus, M., Minasov, G., Shuvalova, L., Inniss, N.L., Kiryukhina, O., Brunzelle, J., Satchell, K.J.F., 2020. High-resolution structures of the SARS-CoV-2 2 2′- O-methyltransferase reveal strategies for structure-based inhibitor design. Sci. Signal. 13, eabe1202.
Ru, J., Li, P., Wang, J., Zhou, W., Li, B., Huang, C., Li, P., Guo, Z., Tao, W., Yang, Y., Xu, X., Li, Y., Wang, Y., Yang, L., 2014. TCMSP: a database of systems pharmacology for drug discovery from herbal medicines. J. Chemin. 6, 13, 13-13.
Rut, W., Lv, Z., Zmudzinski, M., Patchett, S., Nayak, D., Snipas, S.J., El Oualid, F., Huang, T.T., Bekes, M., Drag, M., Olsen, S.K., 2020. Activity profiling and crystal structures of inhibitor-bound SARS-CoV-2 papain-like protease: a framework for anti–COVID-19 drug design. Sci. Adv. 6, eabd4596.
Santiago-Vazquez, Y., Das, S., Das, U., Robles-Escajeda, E., Ortega, N.M., Lema, C., Varela-Ramírez, A., Aguilera, R.J., Balzarini, J., De Clercq, E., Dimmock, S.G., Gorecki, D.K.J., Dimmock, J.R., 2014. Novel 3,5-bis(arylidene)-4-oxo-1-piperidinyl dimers: structure–activity relationships and potent antileukemic and antilymphoma cytotoxicity. Eur. J. Med. Chem. 77, 315–322.
Sharifi-Rad, J., Rayess, Y.E., Rizk, A.A., Sadaka, C., Zgheib, R., Zam, W., Sestito, S., Rapposelli, S., Neffe-Skocińska, K., Zielińska, D., Salehi, B., Setzer, W.N., Dosoky, N. S., Taheri, Y., El Beyrouthy, M., Martorell, M., Ostrander, E.A., Suleria, H.A.R., Cho, W.C., Maroyi, A., Martins, N., 2020. Turmeric and ITs major compound curcumin on health: bioactive effects and safety profiles for food, pharmaceutical, biotechnological and medicinal applications. Front. Pharmacol. 11, 01021.
Shen, M., Tian, S., Li, Y., Li, Q., Xu, X., Wang, J., Hou, T., 2012. Drug-likeness analysis of traditional Chinese medicines: 1. property distributions of drug-like compounds, non-drug-like compounds and natural compounds from traditional Chinese medicines. J. Chemin.-. 4, 31.
Sidhu, G.S., Singh, A.K., Thaloor, D., Banaudha, K.K., Patnaik, G.K., Srimal, R.C., Maheshwari, R.K., 1998. Enhancement of wound healing by curcumin in animals. Wound Repair Regen. 6, 167–177.
Singh, N.A., Kumar, P., Jyoti, Kumar, N., 2021. Spices and herbs: potential antiviral preventives and immunity boosters during COVID-19. Phytother. Res. 35, 2745–2757.
Solis, F.J., Wets, R.J.B., 1981. Minimization by random search techniques. Math. Oper. Res. 6, 19–30.
Sreelakshmi, V., Raj, N., Abraham, A., 2017. Evaluation of the drug-like properties of kaempferol, chrysophanol and emodin and their interactions with EGFR tyrosine kinase - an in silico approach. Nat. Prod. Commun. 12, 1934578×1701200621.
Tao, W., Xu, X., Wang, X., Li, B., Wang, Y., Li, Y., Yang, L., 2013. Network pharmacology-based prediction of the active ingredients and potential targets of Chinese herbal Radix Curcumae formula for application to cardiovascular disease. J. Ethnopharmacol. 145, 1–10.
Tattersall, M.H., Sodergren, J.E., Dengupta, S.K., Trites, D.H., Modest, E.J., Frei 3rd, E., 1975. Pharmacokinetics of actinoymcin D in patients with malignant melanoma. Clin. Pharmacol. Ther. 17, 701–708.
Trott, O., Olson, A.J., 2010. AutoDock Vina: improving the speed and accuracy of docking with a new scoring function, efficient optimization, and multithreading. J. Comput. Chem. 31, 455–461.
Vanommeslaeghe, K., Hatcher, E., Acharya, C., Kundu, S., Zhong, S., Shim, J., Darian, E., Guvench, O., Lopes, P., Vorobyov, I., Mackerell Jr., A.D., 2010. CHARMM general force field: A force field for drug-like molecules compatible with the CHARMM all-atom additive biological force fields. J. Comput. Chem. 31, 671–690.
Veber, D.F., Johnson, S.R., Cheng, H.-Y., Smith, B.R., Ward, K.W., Kopple, K.D., 2002. Molecular properties that influence the oral bioavailability of drug candidates. J. Med. Chem. 45, 2615–2623.
Vellingiri, B., Jayaramayya, K., Iyer, M., Narayanasamy, A., Govindasamy, V., Giridharan, B., Ganesan, S., Venugopal, A., Venkatesan, D., Ganesan, H., Rajagopalan, K., Rahman, P.K.S.M., Cho, S.-G., Kumar, N.S., Subramaniam, M.D., 2020. COVID-19: a promising cure for the global panic. Sci. Total Environ. 725, 138277.
Wang, Q., Wu, J., Wang, H., Gao, Y., Liu, Q., Mu, A., Ji, W., Yan, L., Zhu, Y., Zhu, C., Fang, X., Yang, X., Huang, Y., Gao, H., Liu, F., Ge, J., Sun, Q., Yang, X., Xu, W., Liu, Z., Yang, H., Lou, Z., Jiang, B., Guddat, L.W., Gong, P., Rao, Z., 2020. Structural basis for RNA replication by the SARS-CoV-2 polymerase. Cell 182, 417–428 e413.
Wu, C., Liu, Y., Yang, Y., Zhang, P., Zhong, W., Wang, Y., Wang, Q., Xu, Y., Li, M., Li, X., Zheng, M., Chen, L., Li, H., 2020a. Analysis of therapeutic targets for SARS-CoV-2 and discovery of potential drugs by computational methods. Acta Pharm. Sin. B 10, 766–788.
Wu, F., Zhao, S., Yu, B., Chen, Y.-M., Wang, W., Song, Z.-G., Hu, Y., Tao, Z.-W., Tian, J.-H., Pei, Y.-Y., Yuan, M.-L., Zhang, Y.-L., Dai, F.-H., Liu, Y., Wang, Q.-M., Zheng, J.-J., Xu, L., Holmes, E.C., Zhang, Y.-Z., 2020b. A new coronavirus associated with human respiratory disease in China. Nature 579, 265–269.
Wu, J., Hou, W., Cao, B., Zuo, T., Xue, C., Leung, A.W., Xu, C., Tang, Q.-J., 2015. Virucidal efficacy of treatment with photodynamically activated curcumin on murine norovirus bio-accumulated in oysters. Photo Photodyn. Ther. 12, 385–392.
Xu, X., Zhang, W., Huang, C., Li, Y., Yu, H., Wang, Y., Duan, J., Ling, Y., 2012. A novel chemometric method for the prediction of human oral bioavailability. Int. J. Mol. Sci. 13, 6964–6982.
Yance, D.R., Sagar, S.M., 2006. Targeting angiogenesis with integrative cancer therapies. Integr. Cancer Ther. 5, 9–29.
Yang, X.X., Li, C.M., Huang, C.Z., 2016. Curcumin modified silver nanoparticles for highly efficient inhibition of respiratory syncytial virus infection. Nanoscale 8, 3040–3048.

Yang, X.X., Li, C.M., Li, Y.F., Wang, J., Huang, C.Z., 2017. Synergistic antiviral effect of curcumin functionalized graphene oxide against respiratory syncytial virus infection. Nanoscale 9, 16086–16092.

Yin, W., Mao, C., Luan, X., Shen, D.-D., Shen, Q., Su, H., Wang, X., Zhou, F., Zhao, W., Gao, M., Chang, S., Xie, Y.-C., Tian, G., Jiang, H.-W., Tao, S.-C., Shen, J., Jiang, Y., Jiang, H., Xu, Y., Zhang, S., Zhang, Y., Xu, H.E., 2020. Structural basis for inhibition of the RNA-dependent RNA polymerase from SARS-CoV-2 by remdesivir. Science 368, 1499–1504.

Yu, W., He, X., Vanommeslaeghe, K., MacKerell Jr., A.D., 2012. Extension of the CHARMM general force field to sulfonyl-containing compounds and its utility in biomolecular simulations. J. Comput. Chem. 33, 2451–2468.

Zu, Z.Y., Jiang, M.D., Xu, P.P., Chen, W., Ni, Q.Q., Lu, G.M., Zhang, L.J., 2020. Coronavirus disease 2019 (COVID-19): a perspective from China. Radiology 296, E15–E25.